COMPUTED TOMOGRAPHY PROTCOL OPTIMISATION FOR PEADIATRIC HEAD TRAUMA: RADIATION DOSE AND IMAGE QUALITY ASSESSMENT

This thesis / dissertation is submitted to the University of Ghana, Legon in partial fulfilment of the requirement for the award of **MPHIL Medical Physics degree.**

BY

ANAAFI EVELYN

(10701413)

OCTOBER, 2020

DECLARATION

This thesis is the result of research work carried out by Evelyn Anaafi in the Department of Medical Physics, School of Nuclear and Allied Sciences, University of Ghana, under the supervision of Prof. Albertina Rusandu, Prof. Mary Boadu and Dr. Mercy Afadze.

Sign……..

Evelyn Anaafi

(Student)

Date ……25th May 2021…….

Sign……

Prof Mary Boadu

(Principal Supervisor)

Date……25th May 2021……

Sigr……

Dr. Mercy Afadze

(Co-Supervisor)

Date……10th May, 2021

Sign……

Prof. Albertina Rusandu

(Co-Supervisor)

Date……12th May, 2021

DEDICATION

This research work is dedicated to my parents, siblings, and my family.

ACKNOWLEDGEMENT

I am with a grateful heart thanking the Norwegian Partnership Programme for Global Academic Cooperation (NORPART-project, Ghana-Norway Collaboration in Medical Physics and Radiography Education) and the NORPART coordinators both in Ghana and Norway for given me the opportunity to carry-out this research at the Norwegian University of Science and Technology at Trondheim.

I want to specially thank my most able supervisors with a grateful heart Dr. Mercy Afadze, Medical Physicist, Oslo University Hospital, Prof. Albertina Rusandu, Assistant Professor at the Department of Circulation and Medical Imaging, Norwegian University of Science and Technology and Prof. Mary Boadu, Director at the Radiological and Medical Sciences Research Institute, Ghana Atomic Energy Commission for their marvellous contributions, constructive critics, corrections encouragement and guidance throughout the time of putting together this research. Also, their availability, dedication, love and hard work has made this work completed on schedule. A special appreciation to Sven-Erik Ivan Johnsson, Medical Physicist at St. Olav's Hospital and Atle, Radiographer at St. Olav's Hospital for their support and contribution especially when taking the data for this research.

I am also thankful to Comfort Anaafi, my parents and Prof. JJ Fletcher for always supporting me psychologically and financially.

Finally, a special thank you to all my family and friends especially Kwame Anokye Amoabeng for always being on my nerves to study even when I'm sleeping and Diana Graham who often paid me a visit on campus to release some stress.

TABLE OF CONTENTS

LIST OF TABLES

LIST OF FIGURES

ABBREVIATIONS

2D	Two Dimensional
3D	Three Dimensional
AAPM	American Association of Physics in Medicine
ALARA	As Low as Reasonably Achievable
ART	Algebraic Reconstruction Technique
BW	Beam Width
CNR	Contrast to Noise Ratio
CT	Computed Tomography
CTDI	Computed Tomography Dose Index
DLP	Dose Length Product
DNA	Deoxyribonucleic Acid
eV	electron Volt
FBP	Filtered Back Projection
GCS	Glasgow Coma Scale
ICH	Intracerebral Hematoma
IR	Iterative Reconstruction
kVp	kilo Voltage
mAs	milli Ampere Second
MTF	Modulation Transfer Function
MRI	Magnetic Resonance Imaging
NCRP	National Council on Radiation Protection and Measurements
OPD	Outpatient Department
TF	Table Feed

ABSTRACT

Objectives: To optimise the radiation dose and assess the image quality for a set of protocols, by evaluating noise, contrast to noise ratio, modulation transfer function and noise power spectrum.

Statement of Problem and Justification: Children are sometimes examined with Computed Tomography protocols designed for adults, leading to radiation dose which is higher than necessary. And this can result in radiation induced cancer. Lack of optimisation could lead to image quality higher than what is needed for diagnostic outcome or value of the procedure with associated high dose to patient. Optimising the protocols for paediatric head trauma CT imaging will reduce radiation dose.

Methodology: Somaton Sensation 64 was used to scan the head of an anthropomorphic phantom with a set of protocols. ImageJ software was used to analyse the paediatric head image from the scanner. IMPACTSCAN dosimeter software was used to evaluate the radiation dose to the various organs in the head. MATLAB was used to analyse the Modulation Transfer Function and the Noise Power Spectrum.

Results: The estimated Computed Tomography Dose Index volume ($CTDI_{vol}$) increased with increasing tube current and tube voltage. The high pitch 0.9 gave a lower dose than the 0.5 pitch. Eye lens received the highest radiation dose (39.2 mGy) whiles the thyroid received the least radiation dose (13.7 mGy). There was an increase in noise (62.46) when the H60 kernel was used and a lower noise (8.829) was noticed when the H30 kernel was used.

Conclusion: The results obtained in this work showed that the H30 kernel (smooth kernel) gave higher values for noise and CNR than the H60 (sharp kernel) which values were also high for the MTF and N

CHAPTER ONE

1 INTRODUCTION

1.1 BACKGROUND

The utilization of Computed Tomography (CT) in paediatric imaging has expanded throughout the most recent years and it is quickly expanding since its presentation in 1970s (Stephen et al., 2016). CT uses X-rays to produce images, by combining numerous X-ray projections taken from various directions to get comprehensive cross-sectional images of the body. CT image reconstruction has important effects on image quality and radiation dose (Li K et al., 2014). The CT scanner produces computerized picture that involve a square matrix of a picture element(pixel). The advancement of this modality from single-detector to multi-detector and the possibility for helical scanning has provided many advantages in clinical settings which has made CT the preferred option for several clinical indications (Triantopoulou and Tsapaki, 2017).

In modern times CT embodies about 10% of all ionizing radiation used in imaging modalities, however it deposits more than 50% of the overall collective dose in the diagnostic imaging (Sorantin et al., 2013). From (Gundogdu et al., 2005), the average effective dose for adult cranial CT examination is between 1 and 5 mSv. There is the need for radiation protection since ionization effect has the potential to cause biological damage to tissues.

In direct biological effect, the energy of the photon is imparted into the cells causing the breakdown of both the single and double-stranded helical structures in the deoxyribonucleic acid (DNA). However, when there is breakage in the strands repairing becomes difficult and may lead to cell death. Because the cells of children

are rapidly dividing, they are more responsive and vulnerable to ionizing radiation, there is a need for protocol optimisation and minimization of radiation dose. Simultaneously because of the expanding number of paediatric head CT assessments, comprehensive work has been done to decrease radiation dose in paediatric head CT because of higher danger of radiation initiated malignant growth. Reducing the dose will reduce the absorbed dose but decline the quality of the image.

According to (Hagelstein et al., 2016), tube current reduction based on age, size and weight was formerly used to optimize radiation dose in children. But currently, the use of lower radiation energy is of more interest since it has shown that higher tube voltages have increases radiation in paediatrics without necessarily improving image quality (Trattner et al., 2014).

The practice of as low as reasonably achievable (ALARA) principle thus optimization and justification can result in minimization of unnecessary exposure from CT examinations in paediatric head trauma imaging. Paediatric protocol optimization and review as well as the use of diagnostic reference levels should be enforced to reduce medical exposure in children. Clinical justification is when the benefit of using ionizing radiation surpasses the risk involved. Justifying a CT scan is also very significant in clinical settings

Paediatric head injuries are usually as a result of falls in toddlers and motor accidents and sporting activities on kids. They can be seen in both outpatient department (OPD) or emergency at the hospitals. CT is certified to identify intracranial injuries which needs immediate intervention in cases where symptomatic abusive head trauma or neurological deficit is suspected (O'Brien et al., 2018). The young child, with open sutures and thin flexible calvarium, can absorb traumatic forces better than the older child and the adult.

Currently, CT and Magnet Resonance Imaging are the most accurate non-invasive modalities for showing the morphologic manifestations of the traumatic cerebral process at one point in time. The skull is usually fractured without serious injury to the brain, but the fracture location or type may affect treatment in paediatrics. The parenchymal and extra axial spaces are often depicted with CT examinations.

The level at which CT serves its purpose is directly linked to the quality of the image taken and that has been a major concern in the world of physics. A lot of technical parameters and components in CT affects the image quality. Filtered back projection is the most used image reconstruction algorithm in CT because it is fast and it also intrinsically reduces noise to the image (Andersen et al., 2018). With this the projection data may be corrected prior to back projection. Image quality can be assessed by both objective and subjective methods.

According to (Noferini et al., 2016) CT image quality is a composite of many different factors of both observed and physical quantities like modulation transfer function (MTF), contrast to noise ratio (CNR), uniformity, CT numbers and noise. CNR is the ability to visualise different tissues through noise. MTF determines how much contrast in an original object is maintain by the detector. CT number is the Hounsfield unit. Noise describes any content of an image that limits the ability to visualize lesions or pathology. There is a decrease in noise when CT exposure is increased but at the same time there will be an increase in patient dose. Image quality is how accurately the CT image reproduces the three dimensional attenuation distribution of the X-ray beam through the patient (Zarb et al., 2010). CT image quality is sometimes affected by the image reconstruction algorithms used (Li K et al., 2014).

1.2 STATEMENT OF PROBLEM

The number of Computed Tomography (CT) examinations have increased over the last years due to advances in technology. In paediatrics, the head is the most imaged body part. CT is used to diagnose head trauma and brain injury because of its availability and efficiency in diagnosing injuries that needs to be handled as an emergency case. But the high use of CT has caused great effect of radiation dose, especially in children. Children are vulnerable to ionizing radiation as compared to adults. The practice of ALARA is well established in the developed world, however there is a striking lack of published data regarding such experience in the developing countries (Sodhi et al., 2015). There have been concerns about CT radiation since early 2000s, focusing on paediatric CT with subsequent articles raising concern for potential carcinogenesis from medical imaging (Rogers, 2001).

The effect of ionizing radiation on children can be latent and later cause radiation induced cancer. Therefore, the CT protocols used to image adults should be different from that of children since their cells are more sensitive to ionizing radiation. According to (Naumann et al., 2014), comprehensive CT dose standards exist for adults, but are incomplete for children. It has been a complicated challenge controlling exposure to medical imaging. Paediatric head trauma protocols should be different from other head indications protocols to avoid unnecessary radiation. Much attention should be focused on CT paediatric protocol review and optimisation, to reduce radiation dose.

1.3 OBJECTIVES

The purpose of this research was to optimise CT paediatric head trauma protocols while improving image quality.

The specific objectives of this research work were:

- To optimise the dose and assess the image quality for a set of protocols
- To assess image quality for the set of protocols by measuring noise, contrast resolution, spatial resolution and noise power spectrum and study the effect on radiation dose.

1.4 RELEVANCE AND JUSTIFICATION

Optimising protocols in paediatric head trauma CT would ensure that minimum radiation dose is delivered to the patient while producing image with high diagnostic efficacy. The protocols will be verified which will help the radiographers and medical physicists restructure the radiation protection of paediatric patients in computed tomography examinations across the world through proper application of optimization protocols.

1.5 ORGANISATION OF THESIS

Chapter One deals with the background of the study., the problem statement, objective and relevance of the study. Chapter Two contains the literature review relevant to this research work. Chapter Three describes the research material and methods executed to conduct the study. It will also explain the study design and how the experimental procedures were carried out. In Chapter Four, the experimental results and discussion have been presented. Chapter Five presents the summary, conclusion as well as recommendation and suggestions for further studies.

CHAPTER TWO

2 LITERATURE REVIEW

2.1 COMPUTED TOMOGRAPHY

Computed tomography remains one of the most important diagnostic tools in medicine and health since its inception in the early 1970s by a British engineer named Sir Godfrey Hounsfield and Dr Alan Cormack (Romans, 2011). The advancement of CT has not decreased for the recent years and clinical application continues to grow with increasing benefits to clinicians and patients. CT has greatly, improved patients' comfort because it is fast and painless. CT uses a combination of a computer and X-rays to create images of your bones and tissues, CT shows more details than the conventional X-ray.

The excess of data generated, the expectation of useful image reconstructions by clinical staff, the move to automated segmentation and quantification procedures, sophisticated quality assurance procedures, and the huge potential for excessive patient exposure requires that technological staff are highly efficient and knowledgeable about the opportunities that this device offers (Euclid, 2016). There has been improvement in both CT software and hardware resulting in the advances of its major features like image resolution, temporal resolution, and reconstruction speed. CT uses a narrow X-ray beam that rotates around one part of the body and provide a series of cross-sectional images (slices) from many different angles. These slices are called tomographic images and are more detailed than conventional X-rays. CT scanners also use CT reconstruction algorithms to create a cross sectional picture of the body. CT can be used in diagnosis and prognosis of some medical conditions. Doctors use CT to guide

them during treatment plans and procedures such as biopsies, surgeries, and radiation therapy.

Figure 2.1: A picture of Siemens Somatom 64 slices CT scanner.

2.1.1 X-RAY PRODUCTION IN COMPUTED TOMOGRAPHY

There is a need to know how X-rays are produced to enable us to understand how the CT scan works. X-rays are part of the electromagnetic spectrum with a wavelength from 0.01nm to 10nm, corresponding to frequencies in the range of 30 x 10^{16} Hz to 3x10^{19} Hz and energies from 100 eV to 100 keV. This indicates that X-rays have higher energy than visible light. The amount of radiation dose received during CT scan is less and safe but there is danger in exposure to high doses of radiations.

In an X-ray tube, electrons (projectile electrons) which are formed as a result of thermionic emission in the cathode consisting of a heated filament are accelerated to a focusing cup by a high voltage to impinge on a target that forms part of the anode

(Greg, 2001). X-rays are produced by the deceleration of the projectile electrons by the nuclei of the target material (Bremsstrahlung radiation) or collision with the electrons of the target material (Characteristic radiation).

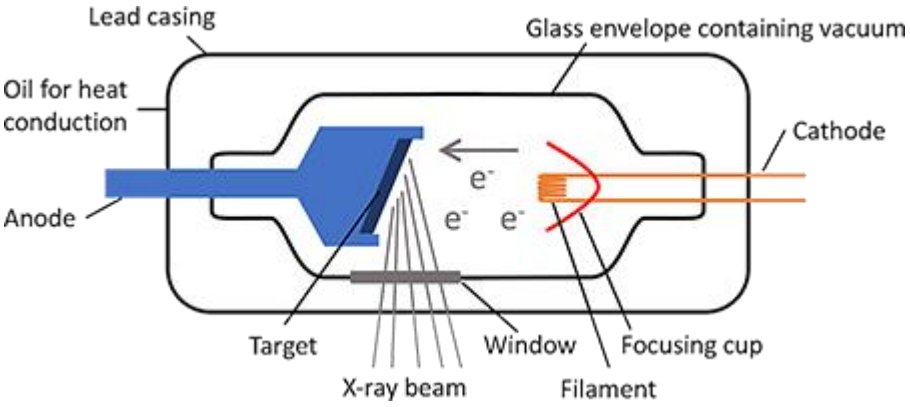

Figure 2.2: A picture of an X-ray tube by radiology café.

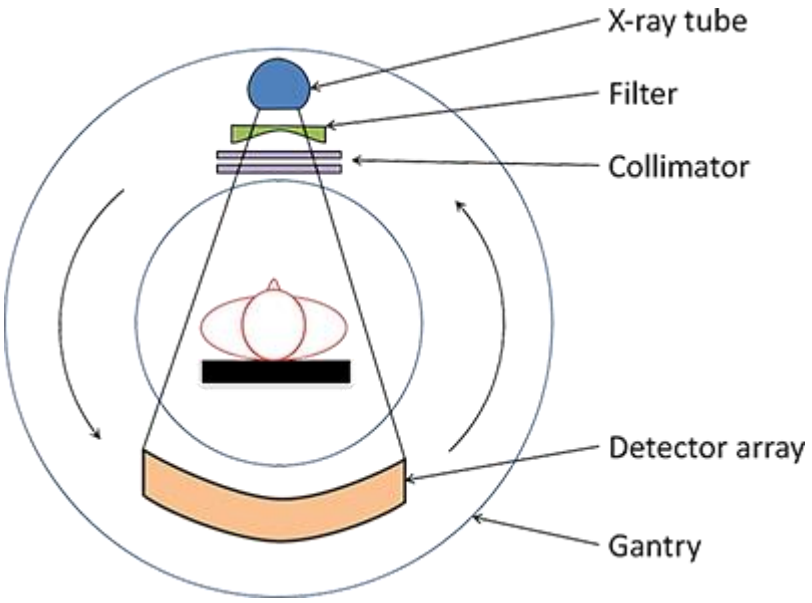

Figure 2.3: CT scanner equipment with a patient being irradiated. Radiology café.

Generally, the metal used for the anode has a high melting point and excellent thermal conductivity to withstand electron bombardment and avoid overheating. Tungsten is the material desirably used for anode construction. According to (Greg, 2001), the X-rays have a maximum possible X-ray energy (in eV) is numerically equal to the

accelerating electric potential, example if the tube is operated at 50 kV then the maximum X-ray energy is 50 keV but usually, the X-ray tubes used in CT are often operated between the potentials of (100 to 150) kV. All X-ray beam sources for CT and conventional radiography produce X-ray energy that is polychromatic.

2.1.2 IMAGE ACQUISITION IN COMPUTED TOMOGRAPHY

CT image is the product of complex calculation based on back projection reconstruction algorithm or iterative reconstruction. During CT image acquisition the tube rotates around the patient body emitting X-rays in a collimated fan beam "slicing" the patient body transversely (Loureiro et al., 2015). A set of projections is obtained when data are acquired by the set of detectors at different source locations.

Helical (Spiral) CT tube is constantly spinning, and the patient table is constantly moving. The ratio of the table feed (TF), that is the table movement per rotation to the beam width(BW) defines the pitch, p, for a helical scan (Smith and Webb, 2011).

$$\mathbf{P} = \frac{TF}{BW} \quad \text{..... (eqn 1)}$$

The radiation energy would be attenuated, and some would pass through the irradiated tissue, when photon beam transvers the human body. The attenuation coefficient μ, determines the attenuation of the material and its dependent on the type of material and the energy of the beam.

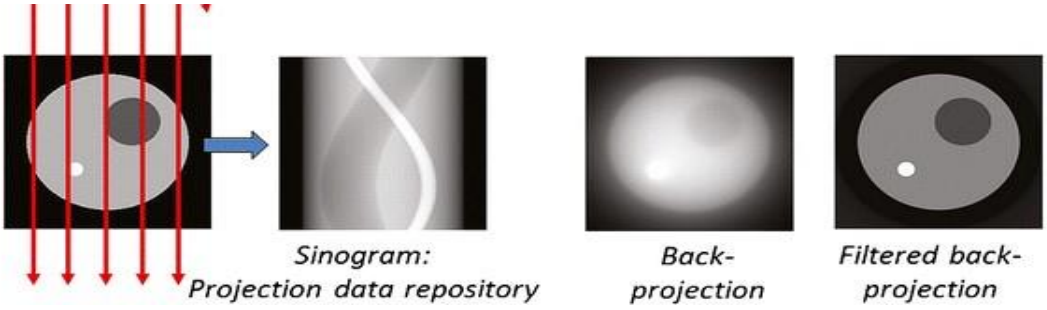

Figure 2.4: Image acquisition in CT from springerlink

A two dimensional image is created from a series of one dimensional image (Smith and Webb, 2011). A projection is obtained by irradiation from one angle. When several projections of the same area have been obtained from different angles, the projection data is usually shown on a sinogram. In the sinogram, the attenuation along a single projection angle is represented by a horizonal line, and the pixel values in the sinogram represent the value of the attenuation coefficients through the objects.

2.2 IMAGE RECONSTRUCTION

A selected body part of the patient is scanned during the CT procedure and the data is reconstructed as cross-sectional images along a selected plane direction. For a given radiation dose it is necessary to reconstruct images with the lowest possible noise without sacrificing image accuracy and spatial resolution.

2.2.1 FILTERED BACK PROJECTION

When generating image from the acquired data involves determining the linear attenuation coefficients of each individual image pixel (Walter, 2016). The intensities from each projection are summed to acquire the reconstructed image. FBP uses a 1D filter on the projection data before back projecting (2D or 3D) the data onto the image space (Yu, 2016). A filter function is applied before the back projection is performed to reduce blurring and artefacts.

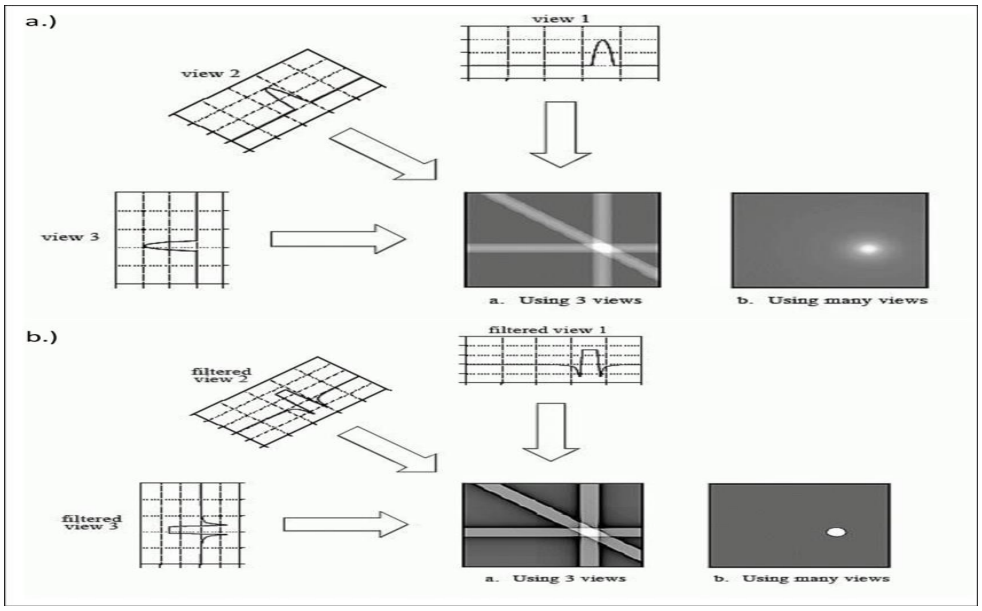

Figure 2.5:

(a) Back projection and (b) filtered back projection of an image using 3 and many projections. dspguide.com

2.2.2 ITERATIVE RECONSTRUCTION

There have been many algorithmic approaches to reduce image noise and artefacts during the image generation over the years. Reconstruction of the first clinical image utilized iterative technique called algebraic reconstruction technique (ART) to invert a large matrix (Hsieh et al., 2013). Unlike the analytical reconstruction algorithms, iterative reconstruction arrives at the final solution in an iterative approach, thus the initial reconstructed images are altered and polished iteratively until certain criteria is met (Hsieh et al., 2013).

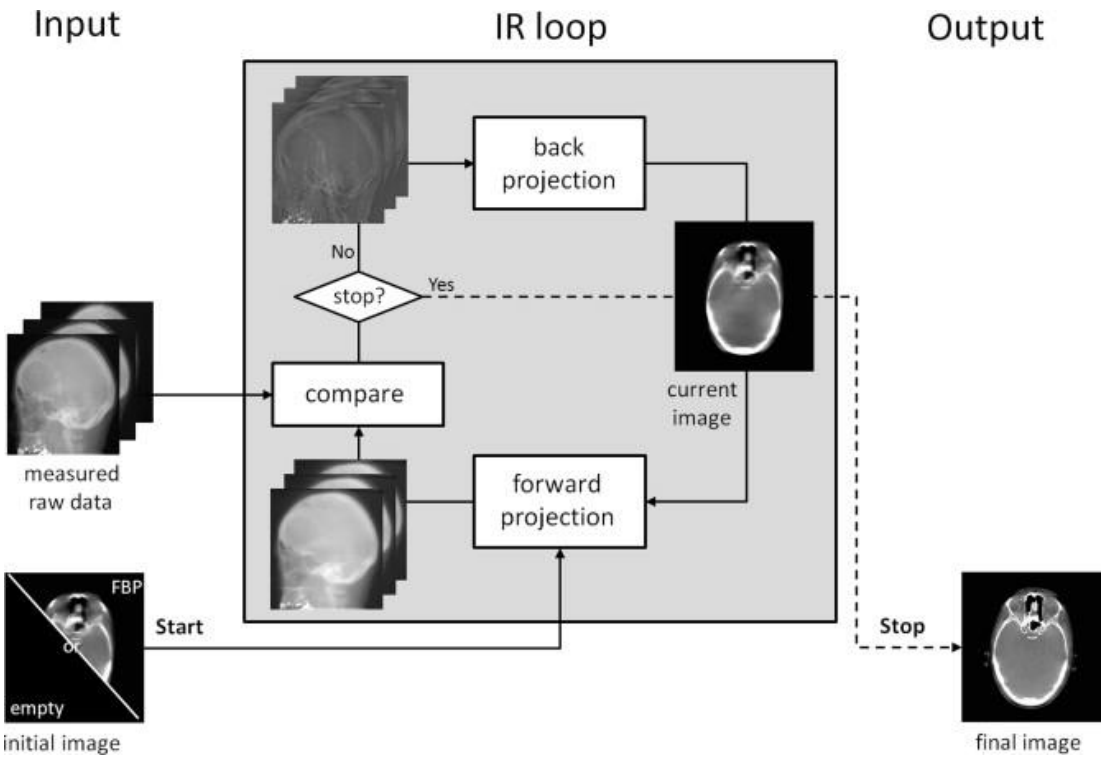

Figure 2.6: The iterative reconstruction is initiated with an empty image estimate information from FBP.

A forward projection of the current image is used to create artificial raw data, which are compared to the real measured raw data. A correction term is used to calculate for the account of differences and then back projected onto the current image to improve the current solution.

2.3 EFFECT OF IONIZING RADIATION ON TISSUE

This describes the probability of short-term and long-term effects of the energy of ionizing radiation in living tissue. Radiation is the emission of particles or electromagnetic wave from a source. When the electromagnetic wave has the energy to eject electron from a neutral atom it is called ionizing radiation. Our body is made up of about 60% of water. The chemical symbol for water is H_2O, meaning two hydrogen atoms and one oxygen atom are bonded together to exist as one water molecule. When there is an interaction with radiation the energy lost by the radiation

is picked up by the water molecule. If the energy gained is strong enough to overcome the bonding force holding the molecule together, the molecule will breakup as shown below:

H_2O -> H + OH

When a radiation splits a chemical bond in this way, it is known as Direct Damage(Burnham, 2005). The damaged produced on DNA by the charged O and OH radicals before combining to form H_2O is called Indirect Damage. The kind of DNA damage determines the effects of the radiation on the cells. The DNA consist of two strands held together by hydrogen bonds. The damage is repairable if there is a single strand break by using the opposite strand as the replacement. Double strand break is more of a problem, they can cause chromosomal breakage that can results in cell death. Non-stochastic effects are deterministic in nature and do not occur below its threshold, severity of the effects increases with increasing dose. Now ICRP-60 has replaced this term of non-stochastic effects by' deterministic effects', examples are erythema, desquamation vomiting and death (Aggarwal, 2014). Stochastic effects on the other hand, do not have a threshold and its probabilistic in nature. Stochastic effects occur due to small exposure received over long period of time that may cause cancer and genetic effects by changing the coded genetic information which causes various deformation, examples are mental retardation, death of the offspring or many other damages (Aggarwal, 2014).

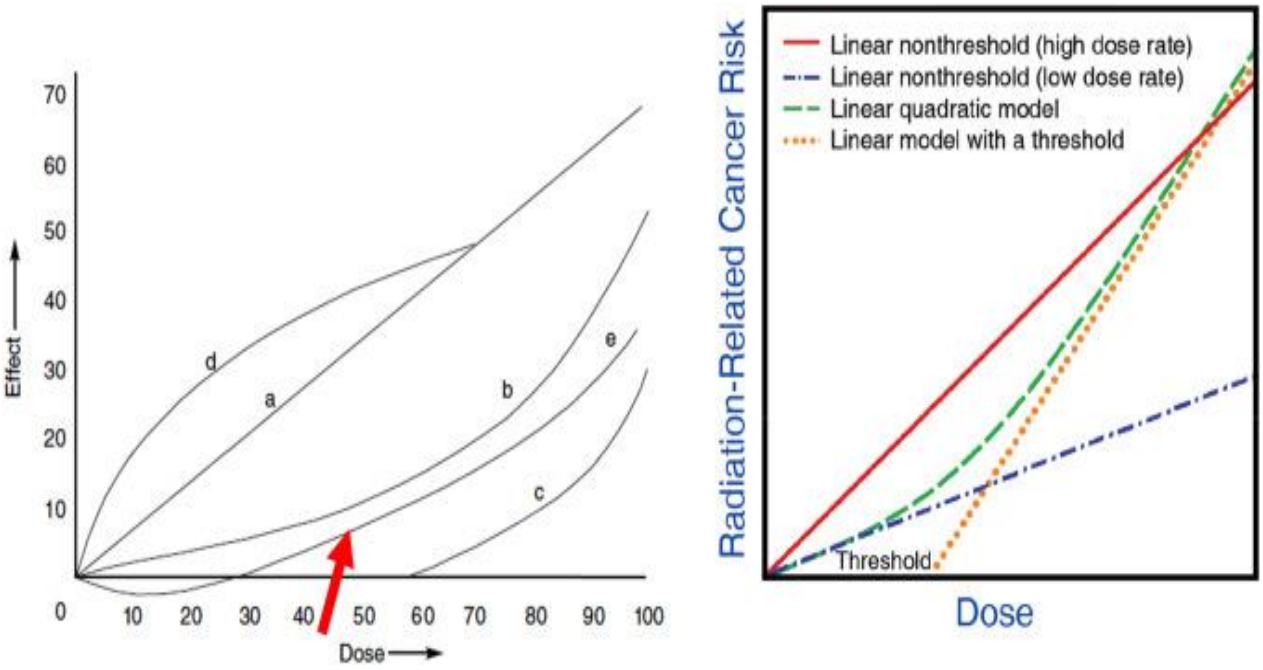

Figure 2.7: This is a graph of linear models of radiation by science direct

To evaluate risk of ionizing radiation exposure, there has been three theoretical dose-response models which have been used. The models used are linear-no threshold model, linear threshold model and linear quadratic model(Bolus, 2001). The linear-no threshold (LNT) model suggests that no matter how low the radiation dose are radiation exposure can induce damage (Seong et al., 2016).

The challenge with this model is that, it does not recognise the role of biological defence in a body and however, assumes that cancer risk occurs in proportionate linear pattern without threshold (Desouky et al., 2015). Upon this limitation the regulatory bodies in medical radiation protection accepts this as the golden standard for radiation risk assessment, and this is because the model ensures maximum protection even at low levels of radiation doses (ICRP, 2007). Linear threshold dose-response model proposed a known threshold below which no effects are seen (Seong et al., 2016). According to (Kim et al., 2005) Linear quadratic dose-response model is used for overall human response to radiation, response at low levels of radiation exposure are

linearly dependent and then become quadratic at higher doses, this model is mainly used in radiotherapy.

Therefore, we are all responsible for the potential biological effects of radiation on children. Children are 10-15 times more sensitive to radiation than older adults (Berenner, 2002). Though the exact excess risk of cancer is not known, it is estimated that a CT abdominal scan results in 1/1000 to 1/5000 excess risk of developing cancer at a later date (Berenner, 2002). There is the need to optimize paediatric radiation dose and enforce the use of the ALARA principle.

2.4 ROLES OF VARIOUS PROFFESSIONALS' IN COMPUTED TOMOGRAPHY

The valuable contribution of CT in medicine was recognised since 1979, when the Nobel Prize in physiology or medicine was awarded jointly to Allan Cormack and Godfrey Hounsfield for the development of "computed aided tomography" as it was originally known (Johnson, 2017).

The role of the diagnostic and therapeutic radiographer in CT has grown over the years. The therapeutic radiographer uses CT simulator to plan radiotherapy treatment. The radiographer is also responsible for radiation protection of patients. According to (SCoR, 2013) the radiographer is involved in each step of the patient pathway, including receiving the referral and justifying or authorising the examination, carrying the exposure, issuing the results and recommending further investigations or follow up care.

The radiographer's role in CT protocol review and management is often perceived as being minimal. The radiographers are given the scan protocols, from the manufacturer and perhaps with some inputs from a physicist who visits once a year. The

radiographer is expected to present his or her perspective on any proposed protocol changes, especially on how the implementation will affect work flow and patient care during CT protocol review session (Trattner et al., 2014). A radiographer who will work long in the hospital is supposed to be designated this duty. The radiographer makes sure that all the new protocols are installed on the CT machines and ensures that the protocols are securely kept and maintained (Trattner et al., 2014).

The radiologist plays a key role as a healthcare provider for patients, especially children. The radiologist is to ensure that every imaging study in paediatric patients is justified, appropriate and indicated for each child. The radiologist influences patient radiation dose through monitoring protocols and targeting body-part and disease-specific protocols that can minimise dose (Trattner et al., 2014). The purpose of selecting protocol is not to get the best technical image quality but to create a diagnostic image with the least amount of radiation dose. Diagnostic radiologists are also now increasingly familiar with the concept of tailoring scan parameters to better match patient size in an effort to reduce dose (Trattner et al., 2014).

The medical physicist plays a lot of significant roles in the diagnostic department. The medical physicist is responsible for patients care by performing acceptance testing, conducting periodic evaluation of diagnostic modalities for regulatory and accreditation compliance, and providing patient dose estimations. Physicist to develop an optimised protocol requires knowledge of clinical requirements, the design and functional characteristics of the equipment, and especially the physical principles and physics that is the foundation of the CT imaging process(Sprawls and Duong, 2013). According to the (AAPM, 2013), the physicist should pay a particular attention to specific capabilities of each individual scanner(examples automatic exposure controls including both tube current and kV selection technologies) to ensure that maximum

performance of the system is achieved. The medical physicist at a time should not be limited to clinical observation and phantom management.

2.5 PEDIATRIC COMPUTED TOMOGRAPHY

There has been rapid increase in the use of CT for paediatric examinations. Paediatric CT is a public health concern because of the potential increased of radiation exposure to children being examined with this diagnostic modality. The risk of using a CT balances the benefit when used appropriately in paediatric case. According to (Amis et al., 2007) approximately 5 to 9 million CT examinations were performed annually on children in the United States. And in 2011, 85 million CT scans were performed in the United States, with 5% to 11% of these scans being performed on children (IMV, 2012).

A study which directly assessed the risk of cancer after CT scans in childhood found a clear dose- response relationship for both leukaemia and brain tumour: the risk increased with increasing cumulative radiation dose (Berrington de Gonzale. A et al., 2009). The effective dose is higher for smaller cross-sectional areas, for any set of CT scanning parameters. Thus, dose is defined as the absorbed energy per unit mass, therefore same amount of energy in a small mass will result in higher radiation dose. For a cumulative dose of between 50 and 60 milli-gray (mGy is a unit of estimated absorbed dose of ionizing radiation) to the head, the investigator reported a threefold increase in the risk of brain tumour (Brenner and Hall, 2007b).

In 2008, the Image Gently campaign was founded by the Society for Paediatric Radiology, the American Society of Radiologic Technologists, the American College of Radiology and the American Association of Physicists in Medicine with the goal of increasing paediatric CT radiation dose awareness by starting a national education and

awareness program (callahan, 2011). The rapidly dividing cells in children are more radiosensitive than those of adults, this increases the risk of experiencing radiation-induced cancer for children and it is because of increasing use of CT.

2.6 PREPARING A CHILD-FRIENDLY AND EXPEDITIOUS COMPUTED TOMOGRAPHY ENVIRONMENT

Healthcare environments are usually cold and unfriendly, diagnostic modality is often intimidating to children and their families (Sze, 2011) . There is a need for paediatric specialists in radiology department, according to (Arthurs et al., 2019) about 75% of children's radiographs and scan are taken in smaller non-specialist hospitals, by radiographers who have no specific training in imaging children and interpreted by radiologists who have less than 6 months' specialist training. Majority of centres (62% in United Kingdom, 90% in Norway for example) still do not have access to 24-hours paediatric opinion (Halliday et al., 2016).

Children should be considered but not as small adult and need care specifically designed for them. According to (Thukral, 2015) techniques and equipment should be employed to minimize the need for sedation (like diazepam, midazolam and ketamine) as it has its own harmful effects. To minimize motion in children use, use distraction tools to improve cooperation and projectors with child-friendly themes, music, toys with flashing light or music, cartoons on the ceiling or walls, singing, counting and parents reading or talking to the child can all reduce anxiety and comfort the child (Strauss ,Goske ,Kaste , et al., 2010). Carefully thought to room design and colours and softening the imaging machine's appearance can potentially change a harrowing experience to more of an experience filled with interest and wonder.

Figure 2.8: a picture of child- friendly environment

This will provide the most precise and least invasive care, in the safest and most cost-effective manner and an environment that provides clarity, warmth and ideally a sense of wonder (Sze, 2011).

2.7 ANATOMY OF THE BRAIN

The head is the upper portion of the body, this consist of the lower jaw and the skull covering and protecting the brain. The head is also attached to the spinal cord by way of the first cervical vertebra.

The brain which is an extension of the spinal cord and they make up the central nervous system which provides sensation, control of movement, reason, emotion, aesthetics, and self-awareness.

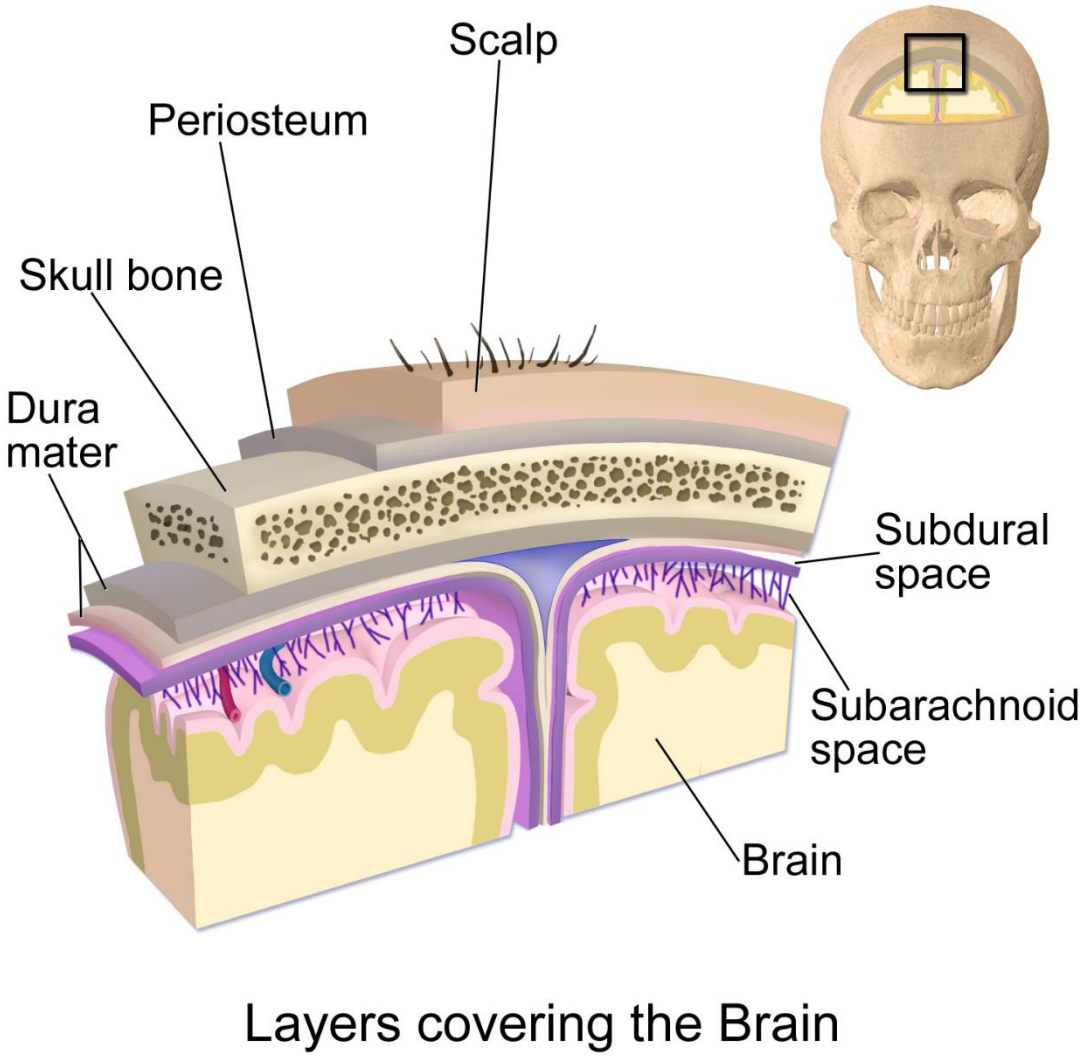

Figure 2.9: Image of the brain by Wikimedia Commons

2.8 PAEDIATRIC HEAD TRAUMA PATHOLOGY

Paediatric traumatic brain injury is one of the leading causes of acquired disability and death in children. The imaging evaluation of the brain injured paediatric patient is directed at detecting the nature of the insults and the evolving pathologic process so that its rate and direction of progression can be determined (Stuart and Shanmuganathan, 2003). Cranial computed tomography is a reliable imaging method for identification of intracranial lesions in patients with head trauma. According to (Syed et al., 2007) traumatic brain injury is a non-degenerative, non-congenital insult

to the brain from an external mechanical force, possibly leading to permanent or temporary impairments of cognitive. The direction and nature of the force that produced injury, the position of the head at the time of injury, and the protection afforded to the brain, example by helmet or degree of ossification at the time of injury are very significant factors in determining the degree of intracranial trauma.

The young child with open sutures and a thin flexible calvarium, can absorb traumatic forces better than the older child and the adult (Stuart and Shanmuganathan, 2003). This flexibility has inherent disadvantages, including allowing severe distortion between the skull, dura and the cerebral vessels to occur. CT delineates the changes that affect the brain parenchyma, subarachnoid spaces, ventricular system and to some extent the cerebral vascular structures. CT can be performed with individual slice scan times of less than one second and, with multi-detector spiral technique, the entire brain can be examined in less than 12 to 15 seconds (Stephen et al., 2016). Traumatic brain injury can be classified using the Glasgow Coma Scale (GCS) which assesses the level of severity and prognosis (Itanyi and HO, 2017). GCS uses patient's best eye, motor and verbal responses in classifying TBI into mild (14-15), moderate (9-13) or severe (3-8). This has prognostic value (Itanyi and HO, 2017).

Skull fracture in paediatric population is often without significant injury to the brain, but the fracture location or type may affect treatment. The pattern of fracturing depends on the location, direction and kinetic properties of the impact as well as intrinsic features of the skull (Raj and Mahapatra, 2012). According to (Stuart and Shanmuganathan, 2003) a depressed fracture over the motor strip or a major dural venous sinus, or significant depression such that the outer table is forced deep to the inner table of the adjacent intact calvarium, may require surgical intervention but CT is the modality of choice for its depiction of the parenchymal and extra-axial spaces.

Subdural hematoma (SDH) in children are similar in imaging characteristics to those seen in adults. SDH is a collection of blood accumulating in the subdural space, the potential space between the dura and arachnoid mater of the meninges around the brain (Jallo and Loftus, 2009). SDH arising primarily within the interhemispheric fissure in infants is often due to "whiplash" or shaken -impact injury, which raises suspicion of non-accidental trauma (Stuart and Shanmuganathan, 2003). It results from extension of intracerebral contusion in the subarachnoid space, causing a greater damage than in epidural hematoma (Alexiou et al., 2011).

Figure 2.10: Epidural hematoma (EDH), is when there is bleeding outside the outermost layer of the dural mater, which is thus stripped off from the inner table of the skull or spinal canal (Pryse-Philip, 2014).

Subarachnoid haemorrhage(SAH) is usually focal, overlying sites of contusion in the interhemispheric fissure paralleling the falx cerebri in children (Stuart and Shanmuganathan, 2003). According to (Hochstadter et al., 2014) SAH was found to be 42% of severe traumatic brain injury patients and was frequently associated with

skull fractures, cerebral oedema, diffuse axonal injury, contusion and intraventricular haemorrhage($p<0.05$).

Cerebral contusion is caused by a direct impact or mechanical damage that causes the brain to strike with the temporal regions of the skull or adjacent neurons (Araki et al., 2017). Contusions are one of the most frequent manifestations of traumatic paediatric brain injury, are often multiple and are often accompanied by other forms of traumatic injuries like acute subdural hematoma.

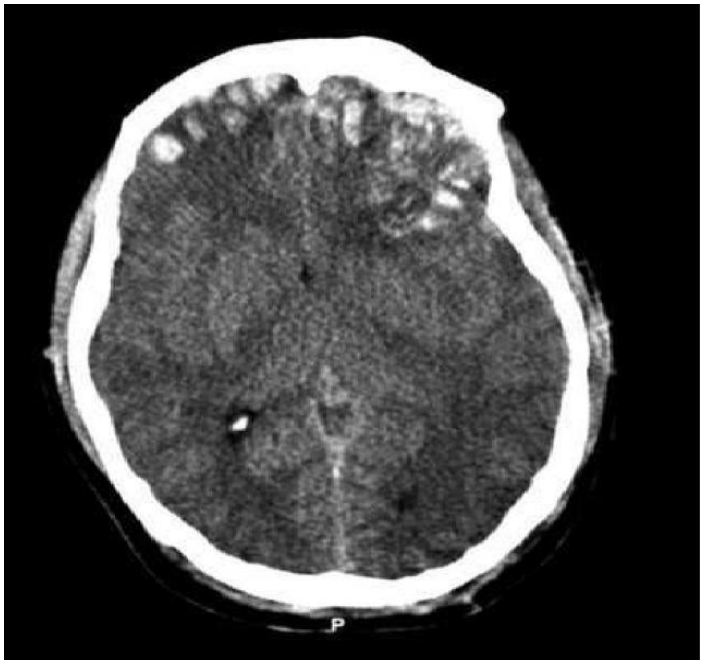

Figure 2.11: Intracerebral hematoma (ICH), are less frequent than contusion but occurs in the same territorial distribution as contusion. They frequently arise in association with contusions, but caused by disruption of larger vessels (Stuart and Shanmuganathan, 2003).

2.9 RADIATION DOSE IN COMPUTED TOMOGRAPHY

There has been a great attention on paediatric radiation dose in journals and reports. Minimization of radiation dose associated with paediatric CT examination is of particular importance because the risk due to radiation exposure is two to three times

greater than the risk to adults (Brisse, 2009). When radiation passes through the body some of it gets absorbed and this contributes to the patient's radiation dose. The X-rays that are not absorbed are used to create the image. Besides the background exposure, medical exposure is the largest source of ionizing radiation exposure to the human population (NCRP, 2009). A recent study indicates that a cumulative dose of 50 mGy triples the risk of leukaemia and a dose of 60 mGy triples the risk of brain tumours in children (Sodhi et al., 2015).

The number of CT cases is 15 % of the total number corresponding to all radiological diagnostic medical devices, the exposure dose is extremely high like 70 % (Choi et al., 2018). Effective dose is the measurement of whole-body radiation dose and the scientific unit is millisievert (mSv). The radiation dose delivered to the examined patient during high dose procedures such as routine CT examinations and image-guided interventional procedures may result in an increased risk of radiation-induced carcinogenesis (Inkoom et al., 2015a). Other radiation dose units are rad, roentgen, gray, rem and sievert. There has been discussion on some design factors that affect radiation dose needed to achieve some particular image quality (Goldman, 2007).

The factors that influences radiation dose can be grouped as equipment related factors as and application related factors. Some of the factors influencing radiation dose are the energy of the beam energy, beam filtration, collimation (section thickness), slice number and spacing, beam shaper and detector array (Nagel, 2007).

Absorbed dose according to (Brenner and Hall, 2007a) is the energy absorbed per unit of mass and is measured in Gray (Gy). According to (AAPM, 2011) the absorbed dose that a patient receives from a routine CT examination is considered to yield very low risk of harm when properly used to obtain a diagnostic benefit. It does not consider where the radiation dose is absorbed or the relative radiosensitivity of the tissue being

irradiated. According to the United States Nuclear Regulatory Commission, a full-body CT gives a dose of 1 rem.

Computed Tomography Dose Index (CTDI) is a standardised measure of radiation dose output of a CT scanner which allows the user to compare radiation output of different CT scanners. CTDI is a dosimetry quantity that is widely used in all CT. CTDI can be used in conjunction with patient size to estimate the absorbed dose. The SI unit of CTDI is milligray (mGy).

Computed Tomography Dose Index over a fixed 100mm length ($CTDI_{100}$) was developed to overcome the limitations of CTDI with 14 sections. The value of $CTDI_{100}$ was over a fixed length of integration using a pencil ionization chamber with an active length of 100mm (Dowsett et al., 2006). This index is defined as:

$$\mathbf{CTDI_{100}} = \frac{1}{NT}\int_{-50nm}^{50nm} D(z)dz \quad \text{..... (eqn 2)}$$

Where N is the number of acquired sections per scan, T is the nominal width of each acquired section and D is the dose.

Weighted version of the Computed Tomography Dose Index ($CTDI_w$) is taking the periphery and centre reading of the head or body phantom, which gives enough basis for specifying reference dose for CT (Dowsett et al., 2006). This index is used to overcome the limitations of $CTDI_{100}$ and its dependency on position within the scan plane. This is represented as:

$$\mathbf{CTDI_w} = \frac{1}{3}\mathbf{CTDI_{100(centre)}} + \frac{2}{3}\mathbf{CTDI_{100(Peripheral)}} \text{ ..... (eqn 3)}$$

Computed Tomography Dose Index volume ($CTDI_{vol}$) is the final CTDI descriptor considers the parameters that are related to a specific imaging protocol, the helical pitch or axial scan spacing (McNitt-Gray, 2002).

$$CTDI_{vol} = CTDI_{w} * NT/I \quad \text{..... (eqn 4)}$$

Dose-Length Product (DLP) is a dose descriptor that is related to CTDI and is commonly reported on CT scanners (M. F. McNitt-Gray, 2002). This value is simply the $CTDI_{vol}$ multiplied by the length of the scan and the unit is mGy.cm. This can be represented as:

$$DLP = CTDI_{vol} * \text{Scan Length} \quad \text{..... (eqn 5)}$$

Effective dose considers where the radiation dose is being absorbed and the radiosensitivity of the tissue irradiated. According to BIER report effective dose allows estimate of stochastic risks. Effective dose is the addition of equivalent doses to all organs, each adjusted to account for the sensitivity of the organ to radiation (ICRPaedia 2007). The SI Unit is millisievert (mSv). Effective dose is the product of equivalent dose to the organs and the appropriate tissue weighting factor. There is a need for tissue weighting factor because all organs have different sensitivity to radiation. Effective dose allows estimate of stochastic risk. Typical values for effective patient dose for some selected protocols are 1-2 mSv for head, 5-7 mSv for chest and 8-14 mSv for abdomen and pelvis (McCollough et al., 2009).

$$E = \sum W * H_T \quad \text{..... (eqn 6)}$$

Organ dose is generally regarded as one of the best metrics to quantify individual radiation burden. Organ dose is essential for patient cancer risk assessment (Gao et al., 2017). Quantifying organ doses in physical phantoms offers a distinct advantage over computational methods because knowledge of the exact photon energy spectrum or irradiation geometry is not required (Winslow et al., 2009).

2.10 IMPACTSCAN DOSIMETRY SOFTWARE

Impact scan dosimetry software is a calculator spreadsheet showing input data from the Toshiba scanner and deriving the effective dose. Mathematical phantom in the impact software is used to simulate CT effective dose. The quality assurance software helps medical physicists achieve confidence that tests are accurate and repeatable. A new version of the CT Dosimetry (version 1.0.4) was made available for download in May 2011 and this is what is used in this research. This version fixes an error with relative CTDI for Siemens Definition AS and add narrow collimation data for the Philips Brilliance 40 and 64. The scanner match data has been incorporated to allow calculation of organ and effective doses to patients undergoing CT scans.

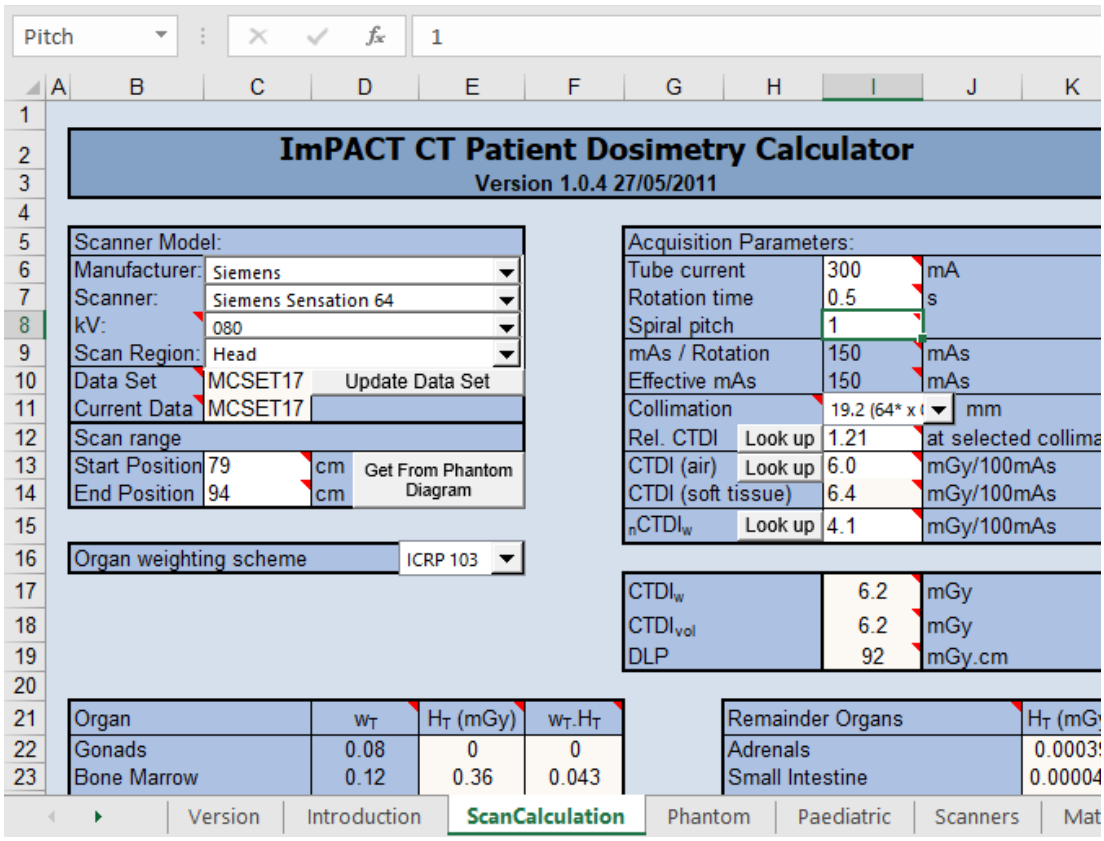

Figure 2.12: An interface of the Impactscan dosimetry calculator.

2.11 COMPUTED TOMOGRAPHY PROTOCOL OPTIMIZATION

Determination of effective dose through organ doses associated with a medical radiation exposure may be considered as the first step in optimising the dose and comparison with diagnostic reference levels (Inkoom et al., 2015b). There remains room for standardization and optimisation for various CT protocols since the CT scanners vary in their capabilities. According to (Trattner et al., 2014) lowest possible mAs (tube current times the rotation time) is proportional to the degree of intrinsic tissue contrast and acceptable level of image noise, so for tissues with high intrinsic contrast, the scan protocols can be adjusted to have very low mAs and still answer the clinical question.

The practice of the justification and optimisation in the ALARA principle can lead to the elimination or reduction of unnecessary or additional radiation exposure associated with the CT imaging is currently relatively well established in the developed world (Sodhi et al., 2015). According to (Kofler et al., 2014) a major challenge protocol review process is determining whether a current protocol is optimal and deciding what steps to take to improve it. There is a great effect of radiation risk on age at higher doses. The appropriateness of the scan associated with technique adjusted to the age and size of the child are important considerations (Morel et al., 2016).

Tube current modulation is one of the techniques to reduce radiation dose. According to (Kalender et al., 2008) the initial efforts on tube current modulation aimed at reducing the tube load by modulating the tube current in a sinusoidal fashion based on the assumption that attenuation in the lateral direction was substantially higher than in the anterior posterior direction. A thorough analysis revealed that attenuation- based TCM allows foe significant dose reduction without any impairment of image quality

and that the current should be modulated following a square root of attenuation relationship for optimal results.

According to the International Atomic Energy Agency, survey of paediatric CT practices in 40 countries published in 2013 show that more than half of the clinical centres relied on machine manufactured protocols and they are set for age groups but research tells that children in the same age group have great variation in body size and composition (Hopkins et al., 2013).

2.12 IMAGE QUALITY ASSESSMENT IN COMPUTED TOMOGRAPHY

Image quality has always been a concern for the medical physics community, it has clinically become more of an issue as strategies to reduce radiation dose especially to paediatric patients as they become a larger focus. According to (Weinman et al., 2019), it is the differential absorption and attenuation of X-ray beams that provides the contrast used in radiographs and CT to distinguish between grey and white matter, haemorrhage and brain. To obtain an image with a higher quality is significant for interpretation and to obtain the highest information from the images. There is a need for knowledge of image quality assessment tools in CT. According to (Zarb et al., 2010) determination of optimal image quality is a complex task involving both quantitative objective physical measures linked with subjective observer perceptions as an indication of clinical performance.

.

2.12.1 Noise

Noise in CT is measured as the standard deviation of voxel values in a homogeneous phantom. Image noise is statistically defined as the standard deviation of CT number or pixel intensity values in a physical uniform region. Noise in CT depends on the

number of x-ray photons falling on the detectors and it is the most important factor affecting the quality of the image (Zarb et al., 2010). There is an increase in image noise when the kVp and mAs are decreased but reduces patient dose. According to (M. McNitt-Gray, 2006), 50% reduction in mAs causes a 40% increase in noise reducing image contrast, but there is a 50% dose reduction thus, CT noise is defined depending on the number of photons received by the detectors. Image noise is inversely relational with the variation square root in the beam thickness(slice thickness) (Alshipli and Kabir, 2017).

2.12.2 Contrast Resolution

Is the ability of an imaging modality to distinguish between differences in image intensity. The low contrast resolution is often determined using objects having a very small difference from background. The low contrast resolution is influenced by CT system specification, milliampere-second, kilovoltage, slice thickness, pitch and beam collimation (Alsleem and Davidson, 2013).

2.12.3 Spatial Resolution

Spatial resolution is the ability to distinguish two separate objects and is directly linked the pixel size, the reconstruction kernel as well as the hardware properties of the imaging modality (Verdun et al., 2015). Spatial resolution depends on the detector width , slice thickness, object to detector distance, focal spot and matrix size (Zarb et al., 2010).

2.13 ANTHROPOMORPHIC PHANTOM

Anthropomorphic phantoms constructed from tissue-equivalent materials have historically been used to provide a physical representation of the body's anatomy and attenuation characteristics for radiation dosimetry studies. The anthropomorphic phantom used in this research was designed to mimic the whole body after 4 years old child of height 105cm. This phantom is a life-size, full body anthropomorphic phantom with a state-of-the-art synthetic skeleton, lung, liver, mediastinum and kidneys embedded in KYOTOKAGAKU original soft tissue substitute. Paediatric whole-body phantom PBU-70 has a weight of 20 kg and can be dismantled. The paediatric anthropomorphic phantoms have been widely used in medical dosimetry (Zhang et al., 2013). Basically, the phantom is designed to be radiographed under same setting as human body, tough, the joints areas may require some adjustment to have better image. Among all radiosensitive organs only the outlines of brain, skeleton and lungs are visible on phantom slices (Inkoom et al., 2015a). Physical phantoms can be used to measure direct radiation dose experimentally (XGEckerman, 2009). Experimental direct radiation dose measurements on anthropomorphic phantoms may be considered more accurate than other methods that use simple phantoms such as a cylinders or sets of slabs (Zhang et al., 2013).

Figure 2.12: Anthropomorphic paediatric whole-body phantom, PBU 70 by supertechx-ray.com

2.14 CATPHAN PHANTOM

Catphan 500/600 is especially designed for evaluation of various image quality parameters in CT and is used worldwide for image quality assurance testing. The quick and easy positioning of the catphan phantom makes it best for routine quality assurance of any CT machine. The catphan phantom's patented design includes many exclusive features that make it easy to achieve perpendicular alignment. Operators find the need of eliminating the repositioning of the catphan since all the test sections are arranged at prescribed intervals from the first module. The integral case mount allows the phantom to be positioned in the scanner, supported off the end of the table, eliminating table artefacts. The catphan 600 model is made from solid-cast materials, eliminating material absorption of water and leaks associated with water bath phantoms. It is constructed from modules that fit snugly into a durable 20cm housing.

The catphan 600, sixth generation model designed to evaluate the maximum performance potential of multi-slice CT scanners.

figure 2.13: Catphan image from research gate

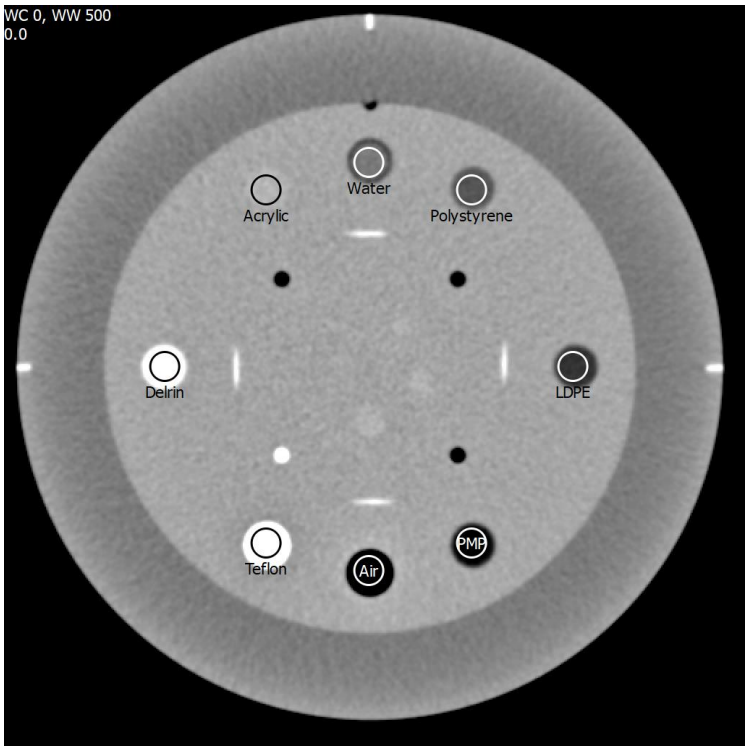

Figure 2.14: Image of the catphan phantom showing the various materials used.

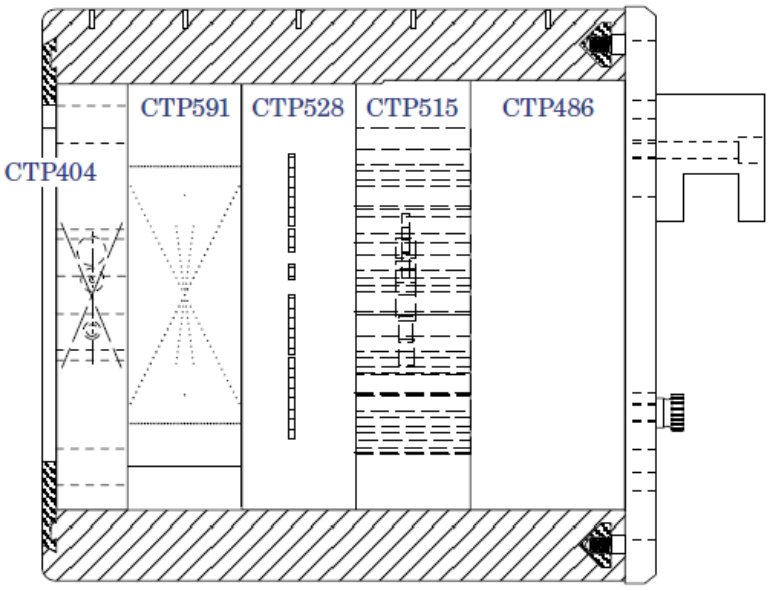

Figure 2.15: Image from catphan 600, the phantom laboratory

The catphan is use to test, scan slice geometry, high resolution (1 to 21 line pairs per cm), phantom position verification, low contrast resolution, spatial uniformity, noise

(precision) of CT systems, sensitometry(linearity), pixel(matrix) size, point spread function and modulation transfer function.

CTP404 has a diameter of 15cm and thickness 25mm. It is used to test the scan slice geometry, phantom position verification, sensitometry, pixel size.

CTP528 has a diameter of 15cm and a thickness of 40mm. it is used to test high resolution, point spread function and modulation transfer function.

CTP515 consist of a series of cylindrical rods of various diameters and three contrast levels to measure low contrast sensitivity.

The CTP486 has a thickness greater than 40mm and does not leak or damage by exposure to freezing temperatures because it does not use water.

CTP591 is the bead geometry module contains both coarse ramps with 1mm z axis increments and precision ramps with 0.25mm z axis increments. It is used to test for slice thickness.

CHAPTER THREE

3 METHODOLOGY

This chapter describes the methodology and the materials used for this work. It discusses, the research design, study area, phantoms, sampling procedure, data collection procedures, data processing and analysis.

3.1 RESEARCH DESIGN

Research design is the glue that holds all of the elements in a research project together, in short it is the plan of the proposed research work (Akhtar, 2016). Quantitative research is used to examine the relationship between variable by using numbers and statistics to analyse and explain its findings. There are four types of which are, descriptive research design, correlational research design, experimental research design and Quasi-experimental research design (Creswell, 2003).

In this work experimental research design was used. Experimental research design according to (Cohen et al., 2007) is when the researcher deliberately controls and manipulates the conditions which determines the events in which they are interested. In this work different scanning protocols that is the kVp and mAs were tested.

3.2 STUDY SITE

This study was carried-out in Norway, Trondheim at the St. Olavs Hospital in their medical imaging department. The hospital serves as the university hospital (Norwegian University of Science and Technology - NTNU) for the medical and research students. It is also integrated with the mid Norway regional health authority and covers a population of 725,600 inhabitants. The department has five computed tomography scanners.

3.3 DATA COLLECTION PROCEDURES

This section gives detailed information on how the data was collected. It entails the CT- scanner used, the anthropomorphic phantom image, the Catphan 600 phantom, Impact scan dosimetry and image quality analysis.

3.3.1 COMPUTED TOMOGRAPHY SCANNER

The CT machine used in this work was the Somatom Sensation 64 manufactured by the Siemens (Figure3.1). The Siemens Sensation 64 slice offers a very high routine isotropic resolution of 0.33 mm, allowing it to visualise the smallest pathology and offers an exceptional 0.24 mm isotropic resolution. The Somatom sensation 64 has an image reconstruction matrix of 512*512 and reconstruction time of 0.06 s per image. It has a maximum scan time of 100 s depending on the pitch, mAs and kVp with a spatial resolution of 30 Ip/cm. The kVp ranges from 80 to 120 and an output power of 80kW. The Somatom sensation 64 uses ultrafast ceramic with adaptive array detector.

Figure 3.1: The Siemens Somatom Sensation 64

3.3.2 PHANTOMS

3.3.3 Catphan 600

The Catphan 600 phantom (Phantom Laboratory Incorporated, USA (Figure 3.2)) was used for the image quality assessment. The Catphan phantom's patented design includes many exclusive features that make it easy to achieve perpendicular alignment. The integral case mount allows the phantom to be positioned in the scanner, supported by the end of the table to avoid artefacts. The easy and fast positioning makes it ideal

for quality assurance programs on every scanner. The Catphan phantom is constructed from modules that fits snugly into a durable 20 cm housing. It is made from a solid-cast material, eliminating material absorption of water and leaks associated with water bath phantoms. The Catphan phantom was used for the objective image quality assessment by measuring the noise, spatial resolution, CT - numbers and contrast resolution.

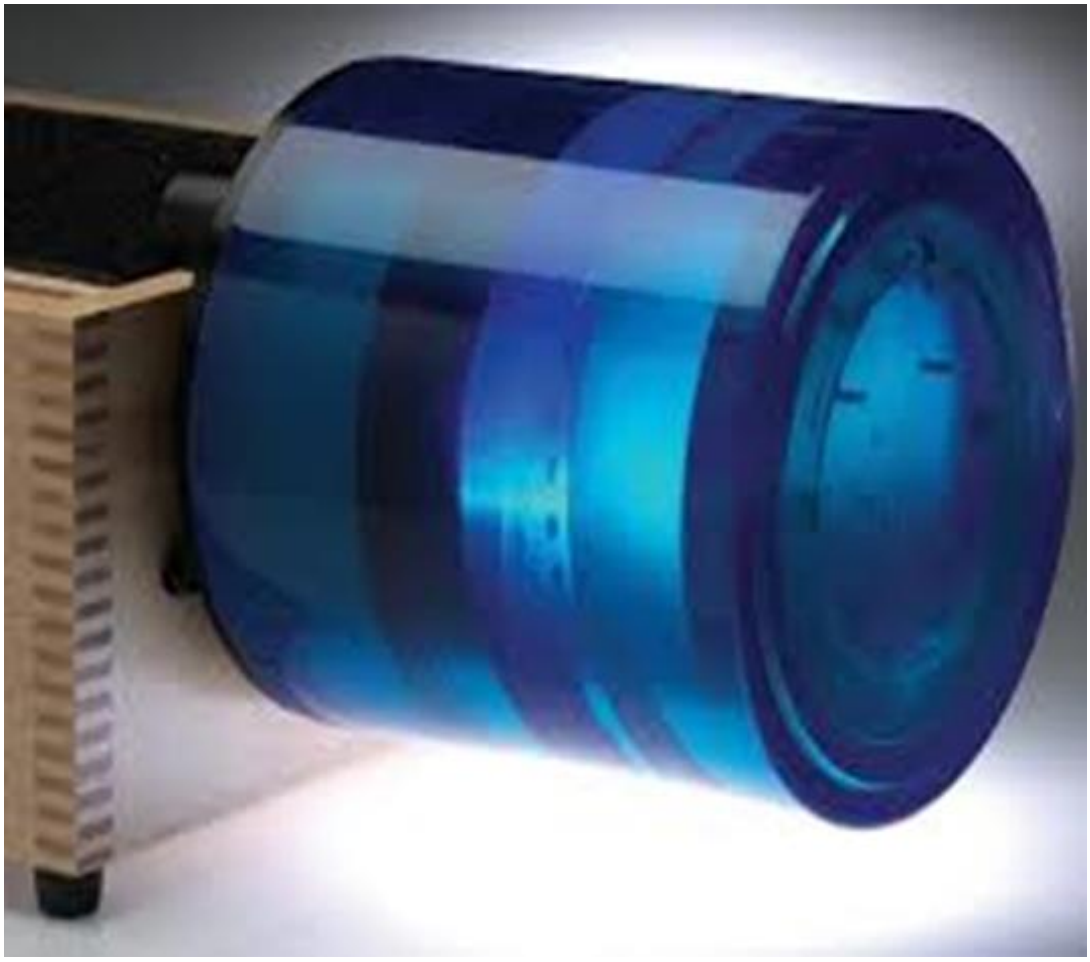

3.3.4 Figure 3.2: Image of the Catphan 600

3.3.5 The Anthropomorphic Phantom

The 5 years anthropomorphic phantom used in this study was manufactured by the Kyoto Kagaku (Figure 3.3). According to (Ramos et al., 2017), anthropomorphic phantoms are built from tissue equivalent materials which represents the anatomy of

the human body and give the attenuation characteristics which enables researchers and physicists to calculate the absorbed dose, improving treatment and protecting healthy tissues. The head of the whole-body phantom PBU-70 was used. The phantom is with the state-of-the-art synthetic skeleton embedded in Kyoto Kagaku original soft tissue substitute.

Figure 3.3: Image of the anthropomorphic phantom.

3.3.6 DATA COLLECTION

The Catphan 600 was positioned on the gantry and the lasers were used to make sure it was well aligned. Twenty-seven (27) test images and one reference image were obtained using different exposure techniques (Table 3.1). H30 kernel was used to smoothen the images and reduce visible image noise and improve contrast resolution. H30 displays body part with inherently small contrast resolution, this gives a better assessment of the brain. High spatial frequency algorithm, H60 kernel was used to

increase the image sharpness at the expense of increased noise. This algorithm is used to display bony parts with inherently wide object contrast. Filtered back projection was used as the post processing algorithm. The field of view used was 210cm and was maintained throughout the work. A slice thickness of 4mm was used for all the exposures with a rotation time of 1s. The reference parameter used was 120kVp and 250mAs which was the protocol from Ghana.

The head of the 5 years anthropomorphic phantom was scanned with the same acquisition protocols used for the catphan.

Table 3.1: Exposure parameters used for acquisition of anthropomorphic and Catphan phantom images

kVp	mAs	Pitch	Slice thickness (mm)
120	250	0.5	4
120	250	0.9	4
120	230	0.5	4
120	230	0.9	4
120	210	0.5	4
120	210	0.9	4
120	190	0.5	4
120	190	0.9	4
100	300	0.5	4
100	300	0.9	4
100	250	0.5	4
100	250	0.9	4
80	300	0.5	4
80	300	0.9	4

3.3.7 $CTDI_{vol}$

Computed tomography dose index volume is a useful patient radiation dose measurement and does not measure the patients absorbed dose. But rather the indicator of dose imparted by the X-ray tube to the patients. A dose sheet is created after the CT scan which shows the average $CTDI_{vol}$ and DLP given by the X-ray tube during the scanning time. In this research the CTDI and the DLP from the scanner was compared with the CT.

3.3.8 Image quality assessment/evaluation

The image quality was assessed using both the subjective and the Objective approach. The radiographer and the medical physicists at the St. Olavs hospital were given the anthropomorphic phantom images to read and assess the quality. ImageJ and matlab were used to calculate the CT numbers, homogeneity, uniformity, contrast to noise ratio, noise power spectrum and the modulation transfer function using the images from the Catphan phantom. Microsoft Excel was used to plot the graphs in this work.

3.4 NOISE

The noise was calculated by setting a region of interest (ROI) of size 40% of the original size on the selected images from the picture archiving communication system (PACS).

$$\textbf{Noise } \alpha \frac{1}{\sqrt{mAs}} \quad \textbf{eqn 3.1}$$

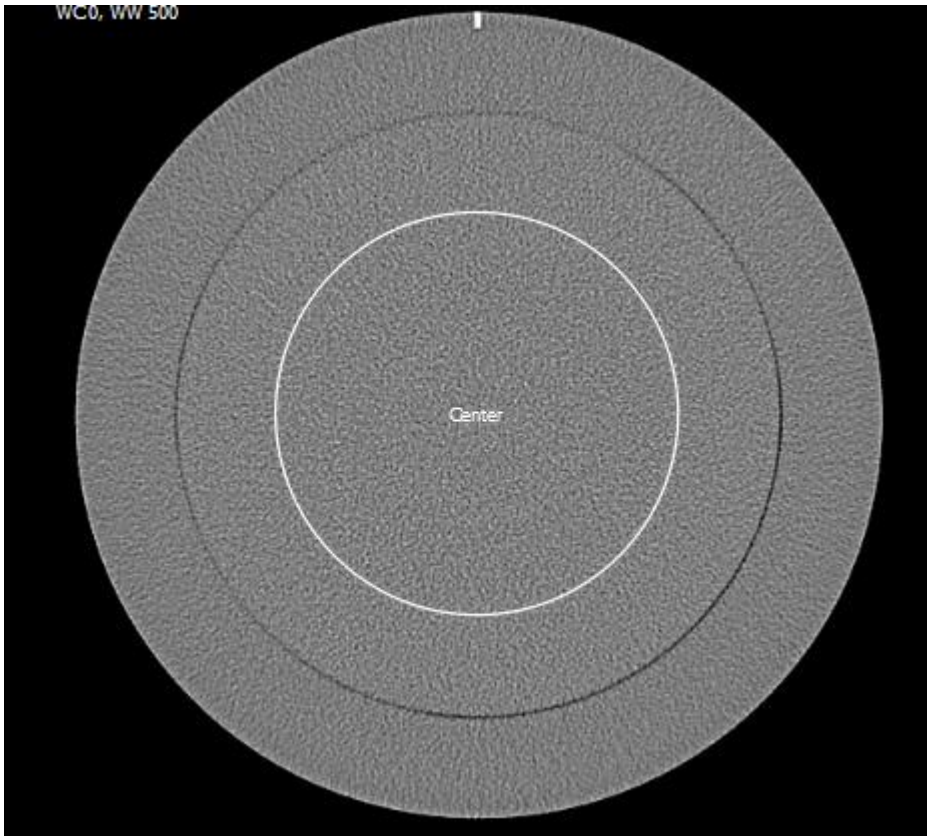

Figure 3.4: Representative image for evaluating noise obtained with the catphan phantom.

3.4.1 Contrast to Noise Ratio

A ROI was drawn in the largest target inside the low contrast module (CTP515). The same size of ROI is drawn close to this target to serve as the background. This was used to calculate the CNR in this work.

Using equation (3.2)

$$\textbf{CNR} = \frac{2(HU_m - HU_b)^2}{SD_m^2 - SD_b^2} \quad \textbf{..... (eqn 3.2)}$$

Where HU_m is the mean HU of the area of interest in the material and HU_b is the mean HU of the background area and SD_m is the standard deviation of the area of interest in the material and SD_b is the standard deviation of the background. A higher CNR, corresponds to a better image quality.

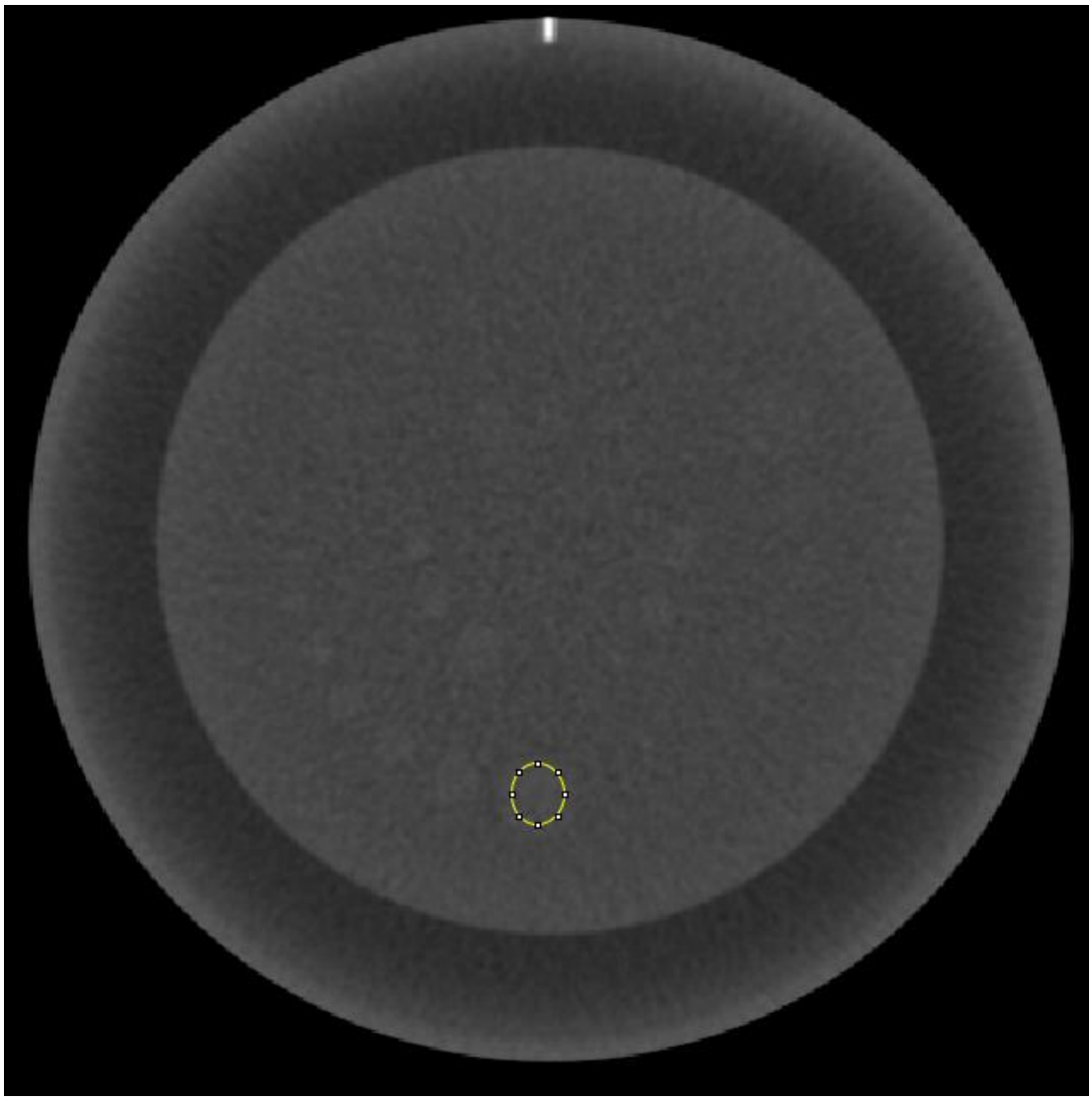

Figure 3.5: A representative image of CNR obtained from the catphan phantom.

3.4.2 CT- numbers

The Catphan phantom has the sensitometry module (CTP404) with inserts of different densities for the measurement of the CT-numbers and linearity. The Catphan 600 has inserts made of Teflon, acrylic, low density polyethylene (LDPE), polymethylpentene (PMP), derlin, polystyrene and air. The CT numbers were measured manually by placing the ROI within the inserts in the CT images.

Figure 3.6: an image of the sensitometry insert in the catphan phantom

3.4.3 MODULATION TRANSFER FUNCTION

The MTF describes the percentage of an object's contrast that is recorded by the imaging system as a function of its size (spatial frequency).

3.4.4 Figure 3.7: an image of the bead in the catphan phantom

3.4.5 Noise Power Spectrum

While noise as the SD in a ROI quantifies the variation of pixel values in a uniform area of an image, it does not give any information about the structure of the noise, that is the graininess of the image in other words, how the image is perceived by an observer. Noise power spectrum is not only affected by the amount of noise present, but also by the noise structure, thus the amount of noise appears as the area under the Noise Power Spectrum (NPS) curve, while the shape of the curve shows characterises the noise structure.

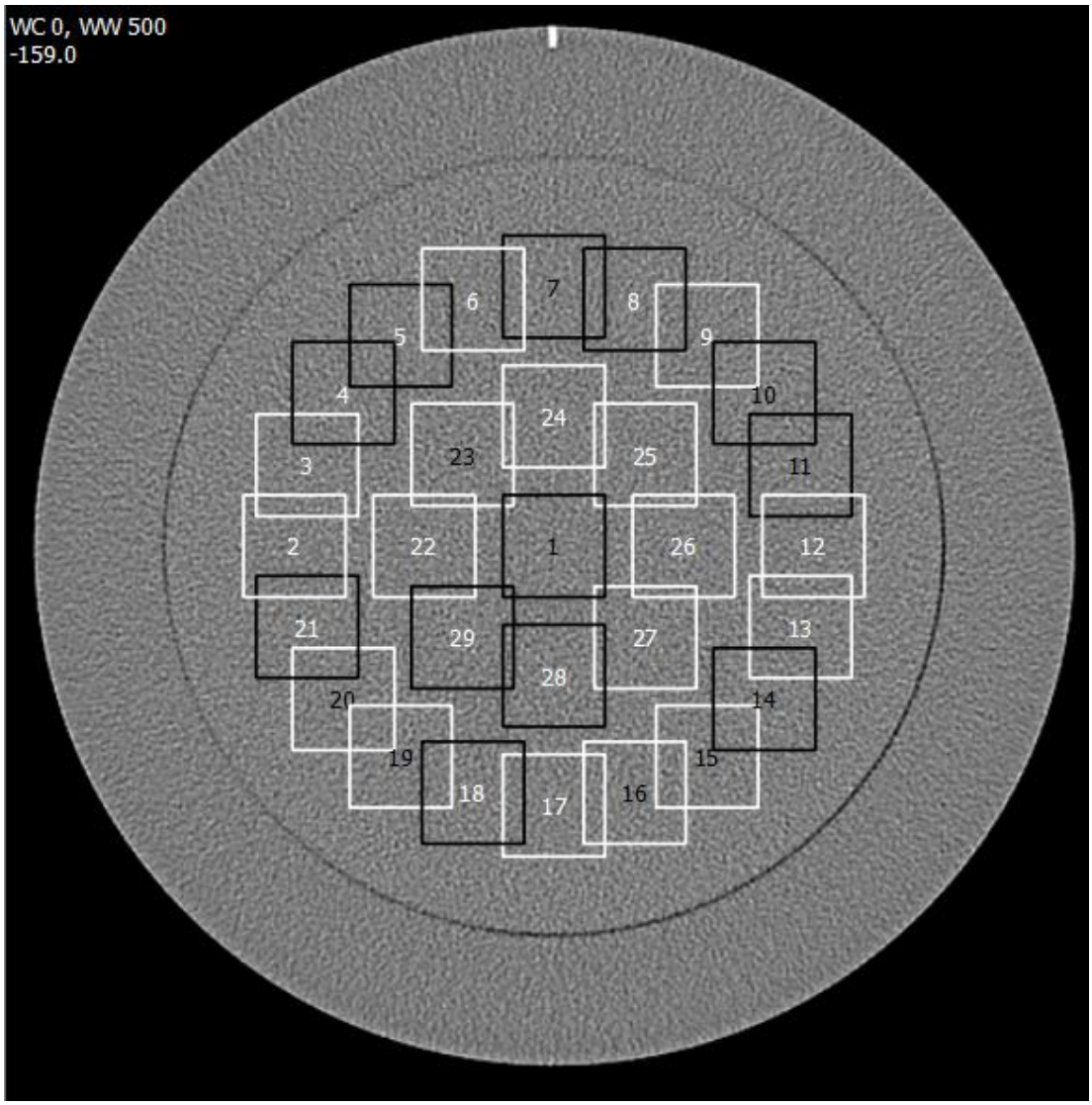

Figure 3.8: An image of uniformity in the catphan

3.4.6 Data Analysis

The data obtained were typed in an excel (2016) sheet for processing and analysis. The IMPACTScan software CTDosimetry (version 1.0.4) was used for the calculation of the $CTDI_{vol,}$ DLP, organ dose and the effective dose. ImageJ version 2.0.0-rc-69/1.52p was use for the analysis of the homogeneity, noise, CT numbers, contrast resolution and spatial resolution, where necessary equations were added example the contrast to noise ratio. A mathematical analysis tool called MATLAB was used to

analyse the noise power spectrum and the modulation transfer function plot graphs used in the data examination.

CHAPTER FOUR

4 RESULTS AND DISCUSSION

This chapter presents the results obtained from this study and discussions thereof. The results include $CTDI_{vol}$, noise, low contrast resolution, noise power spectrum, modulation transfer function and CT number.

4.1 RESULTS OF mAs AND $CTDI_{vol}$ USING A PITCH OF 0.5 AND 0.9

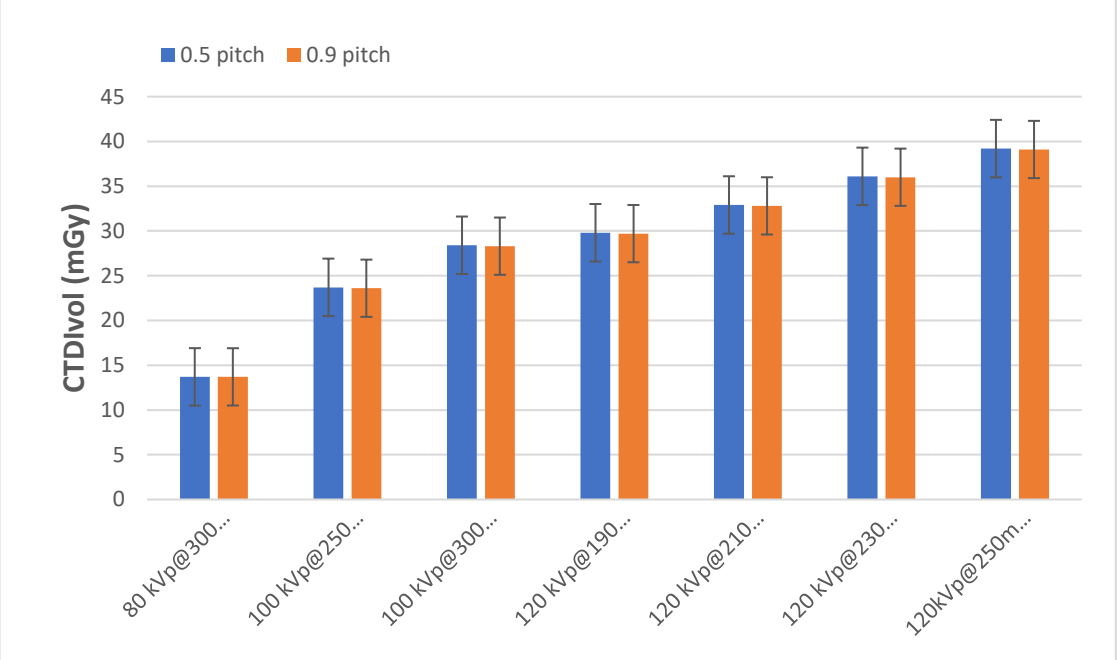

Figure 4.1: A graph of $CTDI_{vol}$ against mAs at 80 kVp, 100kVp and 120 kVp using a pitch of 0.5 and 0.9.

Figure 4.1 shows a graph of increased $CTDI_{vol}$ values with increasing mAs with both pitches of 0.5 and 0.9. This is consistent with (Gundogdu et al., 2005) whose findings was a 50% reduction in mAs produces a 40% increase in noise degrading image contrast and reducing dose by 50%. Additionally, it was observed from the graph that

the 0.9 pitch measured lower dose values by a percentage reduction of 2.3% than the 0.5 pitch. From this study comparing the $CTDI_{vol}$ value of 29.7 mGy at 120 kVp and 190mAs with a pitch of 0.9 to the (AAPM, 2015) paediatric head CT protocols with 120 kVp and 190 mAs and a pitch of 0.85, it was realised that $CTDI_{vol}$ dose of 29.8 mGy was measured using the same type of machine.

From Figure 4.1, there was an average of 39.6% reduction in dose when the kVp was reduced from (120 to 100)kV. A 17% reduction in the mAs decreased the $CTDI_{vol}$ by a percentage of 17%. These findings are in general agreement with (Zaehringer et al., 2016), whose findings came out that a decreased (20%-33%) in mAs produced the same percentage decrease in CTDI and DLP (20%-33%) and confirms the linear relationship between mAs and dose.

Table 4.1: Results of effective dose, DLP and $CTDI_{vol}$

kVp	mAs	Pitch	Eff. Dose (mSv)	DLP (mGy.cm)	$CTDI_{vol}$ (mGy)
80		0.5	0.9	369	13.7
	300	0.9	0.5	205	13.7
100		0.5	2.0	784	23.7
	250	0.9	1.1	436	23.6
		0.5	1.7	654	28.4
	300	0.9	0.9	363	28.3
120		0.5	2.5	1086	29.8
	190	0.9	1.5	603	29.7
		0.5	2.3	999	32.9
	210	0.9	1.3	555	32.8
		0.5	2.1	912	36.1
	230	0.9	1.2	507	36.0
		0.5	1.9	825	39.2
	250	0.9	1.0	458	39.1

It was observed that the DLP was decreased by 87 mGy.cm with the tube voltage of 120 kVp and reducing mAs from 250 to 190 with an interval of 20 mAs when the pitch was 0.5 but the DLP reduced by 48 mGy.cm when the pitch was 0.9. The average DLP for the 0.5 and 0.9 pitches were 804.143 mGy.cm and 446.714 mGy.cm respectively. These values show a 44.4% reduction in the 0.9 pitch. There is significant

difference. The lowest dose 205 mGy.cm was recorded at 80 kVp and 300 mAs using a pitch of 0.9 and this is because DLP is a product of CTDI and length so with constant length, the lowest $CTDI_{vol}$ will give the lowest DLP.

4.2 RADIATION DOSE AND IMAGE QUALITY

4.2.1 NOISE

Figures 4.3A shows a graph of noise and $CTDI_{vol}$ using H30 and H60 kernels with a pitch of 0.5.

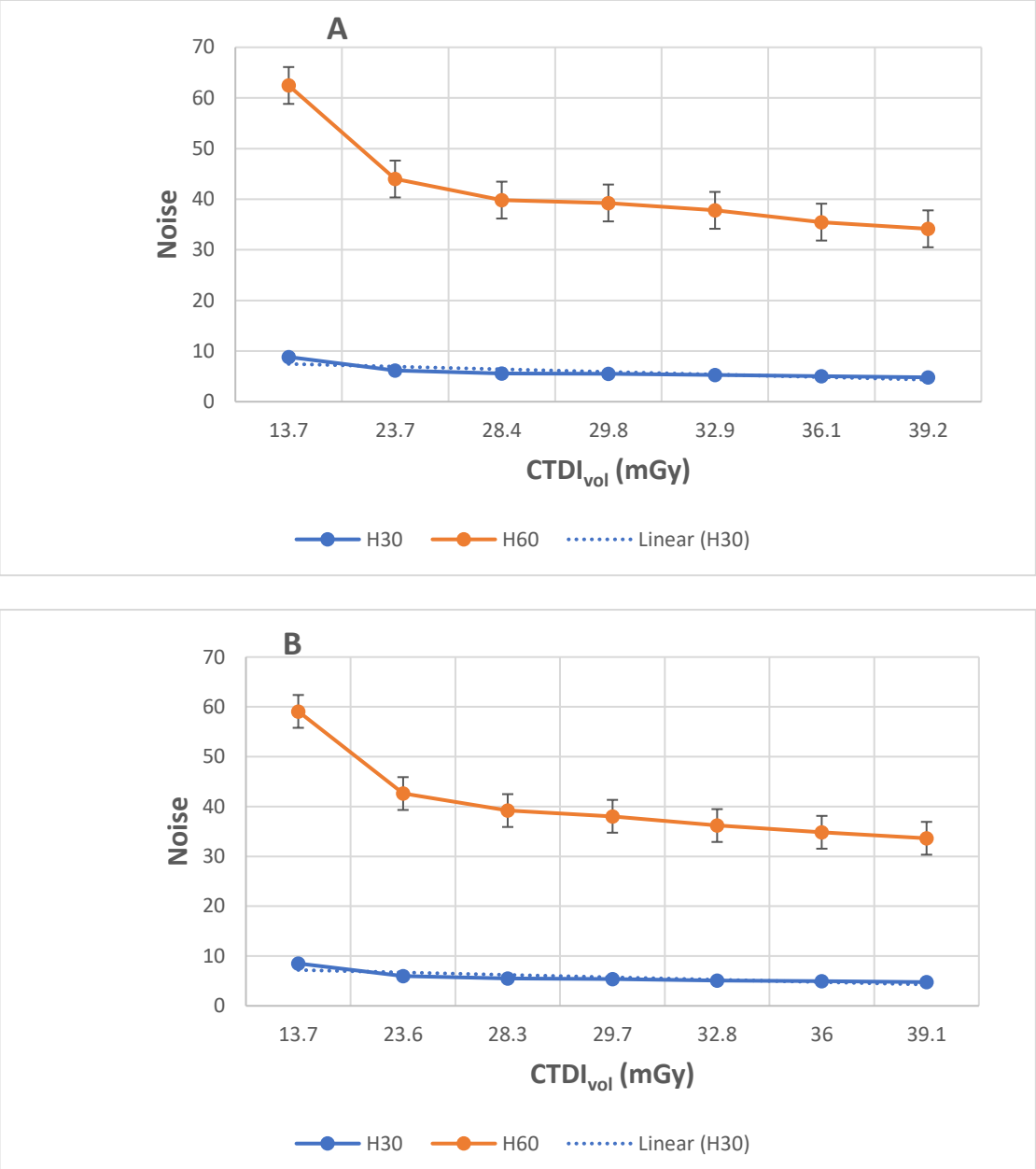

Figure 4.2: A graph of noise and $CTDI_{vol}$ using H30 and H60 kernel with (A) a pitch of 0.5 and (B) a pitch of 0.9.

Increasing the $CTDI_{vol}$ reduces the noise in the image as illustrated in Figures 4.2A and 4.2B. The mAs determines the number of photons reaching the detector. Noise in

CT depends on the number of X-ray photons falling on the detectors referred to as quantum noise and is the most important factor affecting the quality of the image (Zarb et al., 2010). Comparing the H30 and H60 kernels there is a significant difference in noise. There is an average of 83.6% increase in noise when the kernel was changed from H30 to H60. Additionally, this shows that the sharp kernel (H60) is not good for imaging organs with low contrast organ like the brain since it produced image with more noise.

It was also observed from Figure 4.2A that, there was an increase in noise as dose decreases in both the H30 and H60 kernels which reduces image quality. This agrees with (Choi 2018), whose findings stated that a decrease of the dose in a paediatric abdominal CT scan will cause a high level of noise and reduce image quality. In addition, there was nearly no change in the noise (5.593) at 28.4 and 29.8 mGy as $CTDI_{vol}$ increased. There was a significant difference in the noise as the kernel was changed from H30 to H60.

From Figure 4.2B, the same results in Figure 4.2A was observed with, the H30 kernel given a lower noise as compared with the H60 kernel. However, there was no significant difference in noise when the pitch was changed from 0.5 to 0.9.

There was an average of 2.3% reduction in $CTDI_{vol}$ when the pitch was changed from 0.5 to 0.9. There was a strike balance between noise (5.49) and $CTDI_{vol}$ at 28.3 mGy

4.2.2 CONTRAST TO NOISE RATIO

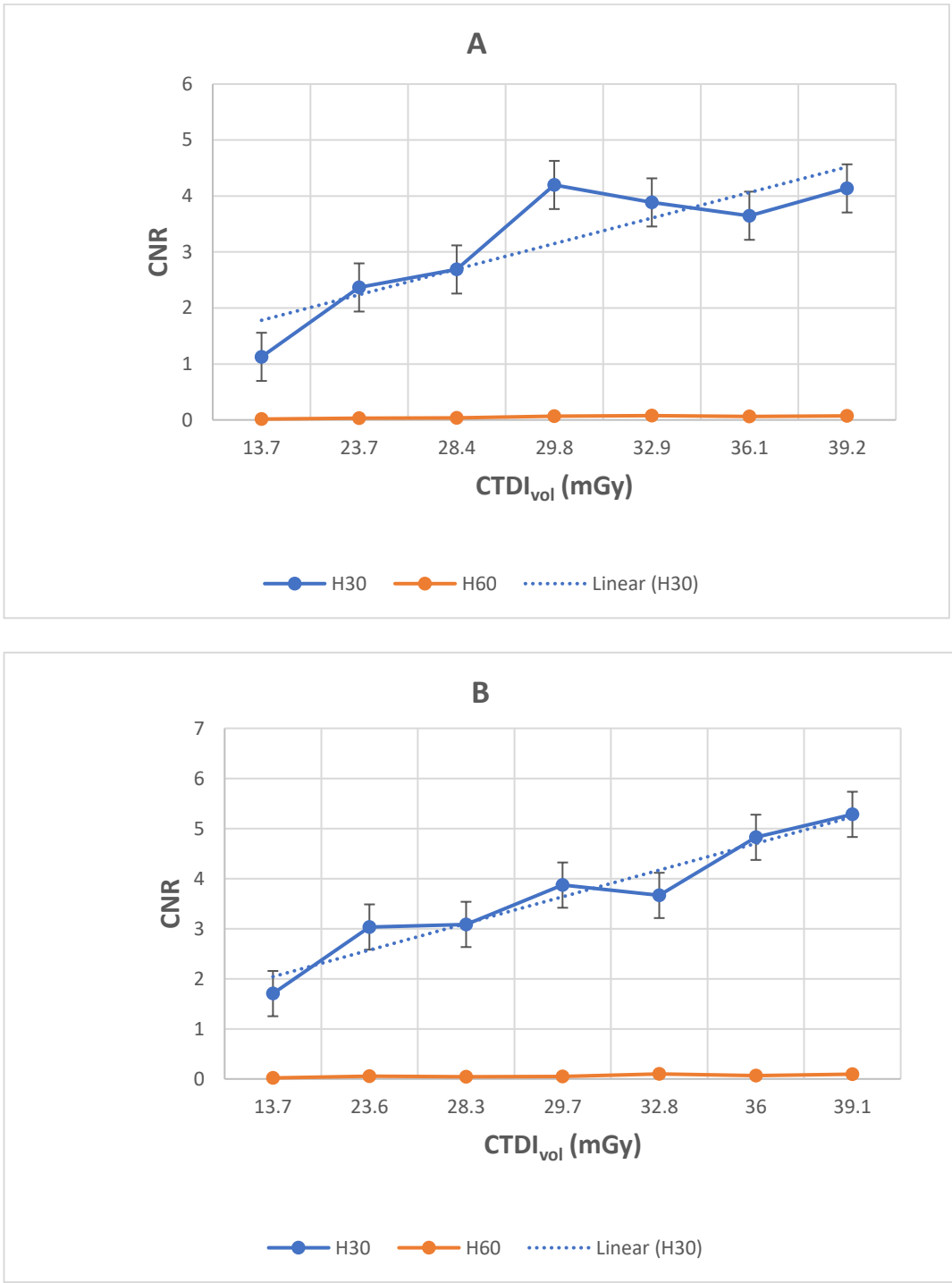

Figure 4.3: A graph of CNR and $CTDI_{vol}$ (mGy) using H30 and H60 kernels (A) with a pitch of 0.5 and (B) with a pitch of 0.9.

In Figure 4.3A, a steady increase in CNR was observed with increasing $CTDI_{vol}$ but decreased after 29.8 mGy at the CNR increased. CNR is greatly degraded by noise, hence, a decrease in $CTDI_{vol}$ will lead to a decrease in CNR due to increase noise at lower doses. Generally, lower kVp enhances CNR, nevertheless, the lowest CNR was recorded at the lowest kVp in this study. This is the lowest $CTDI_{vol}$ was observed with at the lowest kVp as seen in Figure 4.3. Additionally, an average of 98% decrease in CNR was observed when the kernel was changed from H30 to H60. This agrees with (Yu, 2016), who estimated that the CNR is largely affected by the reconstruction technique used and may be influenced by the detectability of pathology. The H30 kernel with higher values of CNR indicates that it is better to use the H30 kernel when imaging the brain, because of the low contrast in the brain tissues.

The CNR determines the contrast detail that can be visibly reproduced when there is a small difference in density relative to the surrounding area, implying that more subtle objects can be seen on the image. There was not much significant change in the CNR when the pitch was increased from 0.5 to 0.9 although the 0.9 pitch gave a slightly higher CNR value than the 0.5 pitch. Furthermore, at constant kVp, it was observed that the value of CNR increased as the tube current (mAs) increased except at 210 mAs, this did not agree with the findings of (Choi, 2018), who estimated that the value of CNR increased as tube current increases in all diameters of the phantom.

In Figure 4.3A, the H60 kernel measured lower values of CNR than the H30 kernel which measured a significantly higher CNR values. The H60 kernel showed a linear increase in $CTDI_{vol}$ with no significant change in the CNR. The H30 kernel increased non-linearly in the CNR values as the $CTDI_{vol}$ increased.

The results in Figure 4.3A, is similar to the results in Figure 4.3B. H30 kernel measured a higher CNR value than the H60 kernel.

Furthermore, at a CNR value of 5.282 and a $CTDI_{vol}$ value of 39.1 mGy there was a strike balance between image quality and radiation dose.

From Figures 4.3A and 4.3B there was a 26.6% reduction in dose when the protocol was reduced from 120 kVp 250 mAs to 120 kVp 190 mAs.

4.2.3 MODULATION TRANSFER FUNCTION

A graph of MTF and $CTDI_{vol}$ with a pitch of 0.5 and H30 and H60 kernels are presented in Figures 4.4A and 4.4B respectively using spatial frequency of 50% and 10%.

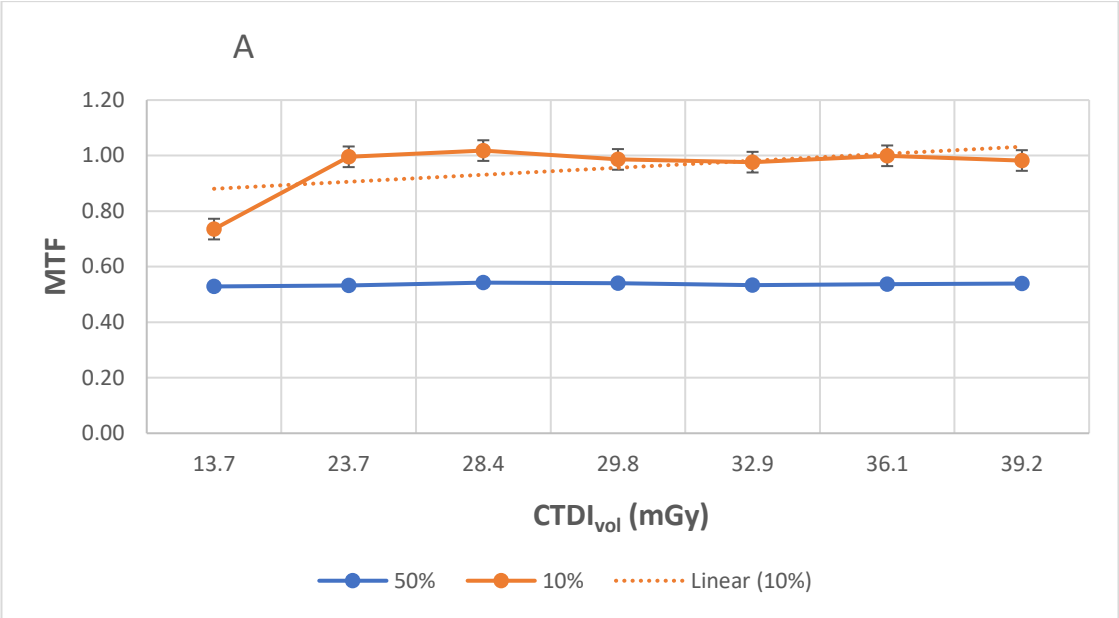

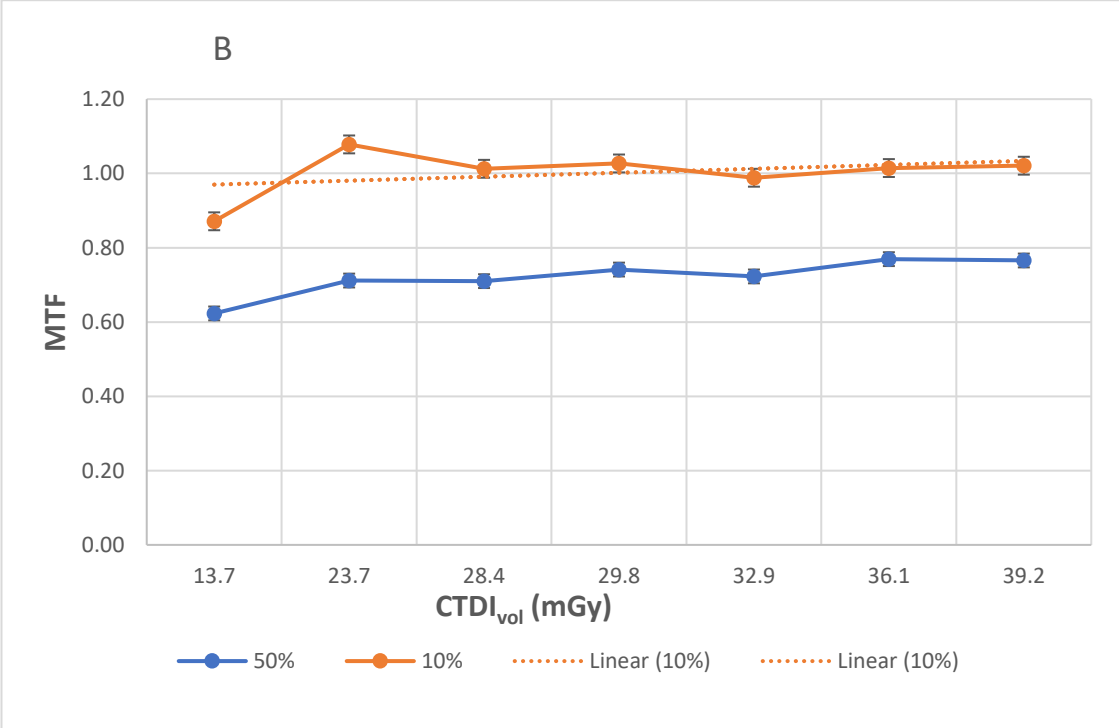

Figure 4.4: A graph of MTF and $CTDI_{vol}$ with a pitch of 0.5 using

(A) H30 kernel and (B) H60 kernel.

From Figure 4.4A, at 50% spatial frequency, MTF was constant as the $CTDI_{vol}$ increases. While at 10% the MFT sharply increased to 1.08 at 23.7 mGy $CTDI_{vol}$. However, there was no significant variations in MTF (1.02 to 0.98) when the dose was increased from (28.4 to 39.2) mGy. From Figure 4.4B, there was no variation in MTF

at 50% spatial frequency with dose. While at 10% there was a steady increase in MTF as the $CTDI_{vol}$ increased was observed. Additionally, there was no clear change in the MTF values.

A graph of MTF and $CTDI_{vol}$ with a pitch of 0.9 and H30 and H60 kernels are presented in Figures 4.5A and 4.5B respectively using spatial frequency of 50% and 10%.

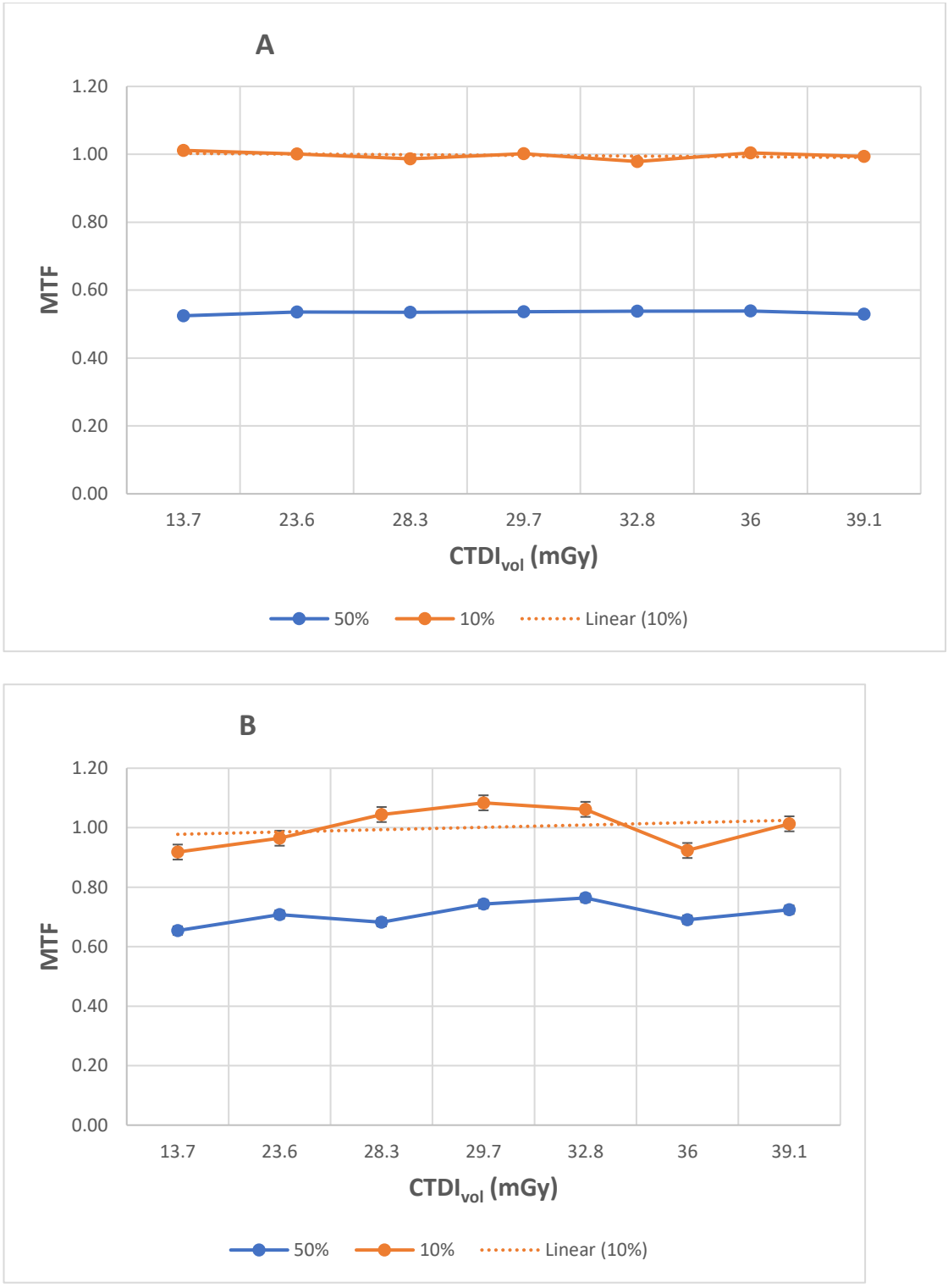

Figure 4.5: A graph of MTF and $CTDI_{vol}$ with a pitch of 0.9 using (A) H30 kernel and (B) H60 kernel.

From Figure 4.5A, both the 10% and 50% spatial frequency appeared to be linear with no significant difference in MTF. Additionally, Figure 4.5B showed an increase in

image quality for both spatial frequencies from 13.7 mGy to 29.7 mGy and slowly decreased at 32.8 mGy. Moreover, there was a sharp decrease at 36mGy and increased at 39.1 mGy. There was no change in MTF value after 1.08 and radiation dose at 29.7 mGy.

Figures 4.5A and 4.5B give a clear indication that the H60 kernel (sharp kernel) gave a higher MTF values than the H30 kernel (smooth kernel), this indicates the sharp kernel has better spatial resolution than the smooth filter. This is good for imaging bony structures. Since the head is made of soft tissues and bony tissues. To visualise fracture in bone, the H60 will be more appropriate. Additionally, the reconstruction kernel used affects the ability of the imaging system to differentiate objects in the two spatial dimensions of an image. Furthermore, at 10% there were higher MTF values than at 50%, this also proves that the spatial frequency affects the MTF.

4.2.4 NOISE POWER SPECTRUM

Figure 4.6 shows a graph of normalised noise and spatial frequency with a pitch of 0.5 and 0.9 using H30 and H60 kernels.

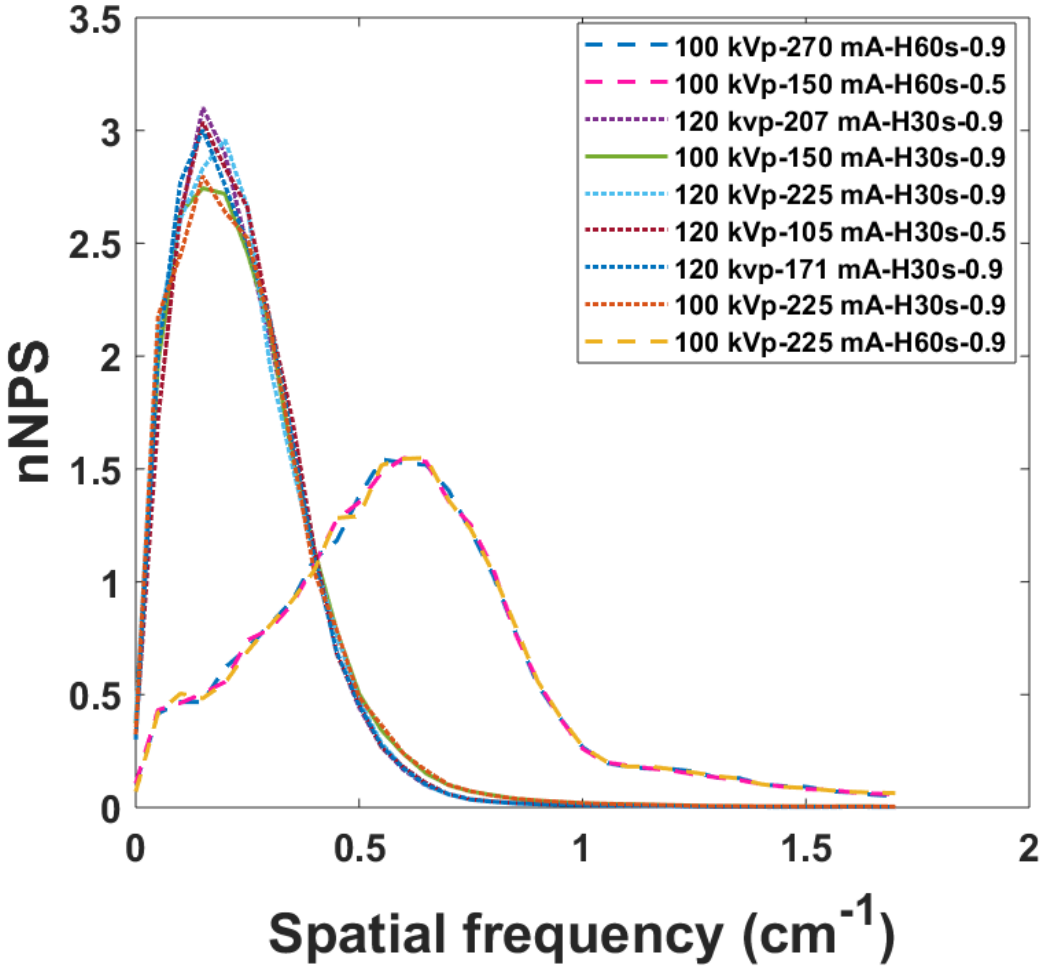

Figure 4.6: A graph of nNPS and spatial frequency.

From the Figure, it was observed that the H60 kernel was skewed to the right while the H30 kernel was skewed to the left. This implies that, the H60 kernel had sharper images even though they were noisier. Thus, the closer the NPS peak is to the right, the sharper the image appearance, in other words, the images will have fine grainy appearance. The H30 kernel had lower NPS value and the images appeared smoother but were not sharp. This is good for imaging bony structures. Since the head is made

of soft tissues and bony tissues. To visualise fracture in bone, the H60 will be more appropriate.

4.3 RESULTS OF ORGAN DOSES USING DIFFERENT PITCH

Figures 4.7A and 4.7B gives the results of organ doses using a pitch of 0.5 and 0.9 respectively.

A tube voltage of 120 kVp and tube current of 190, 210, 230 and 250 mAs were used for the two different pitches.

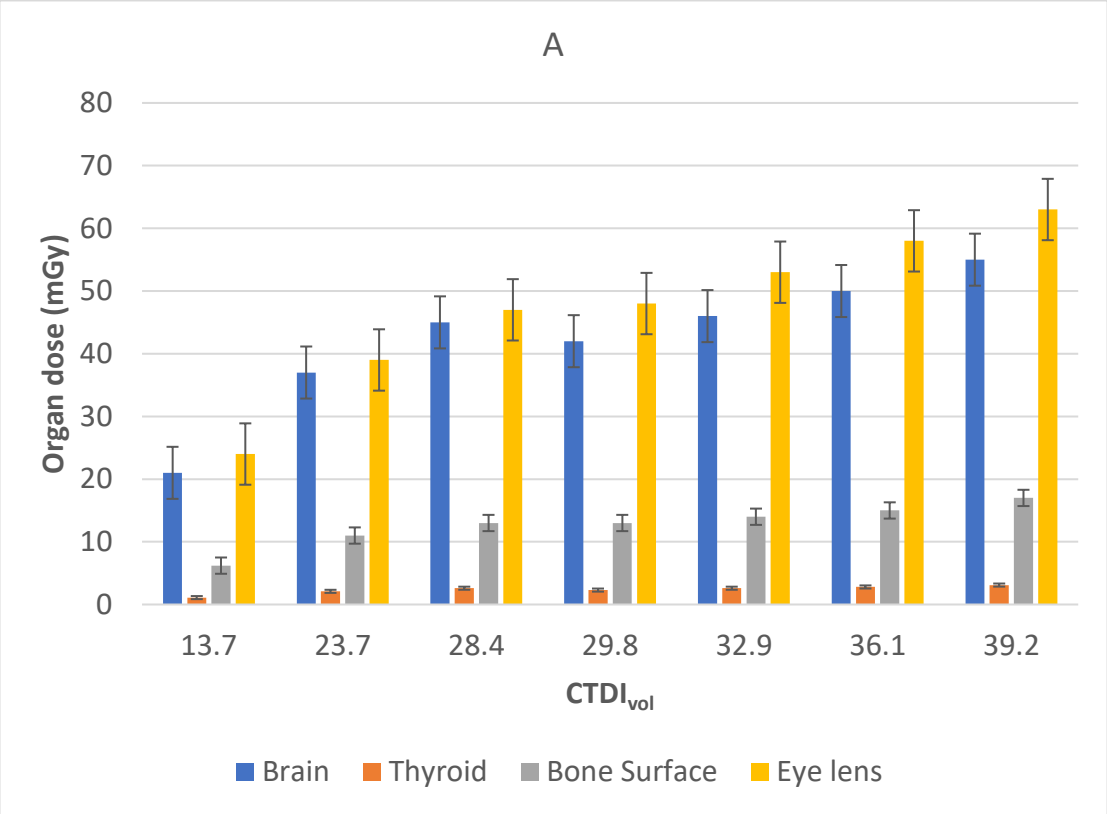

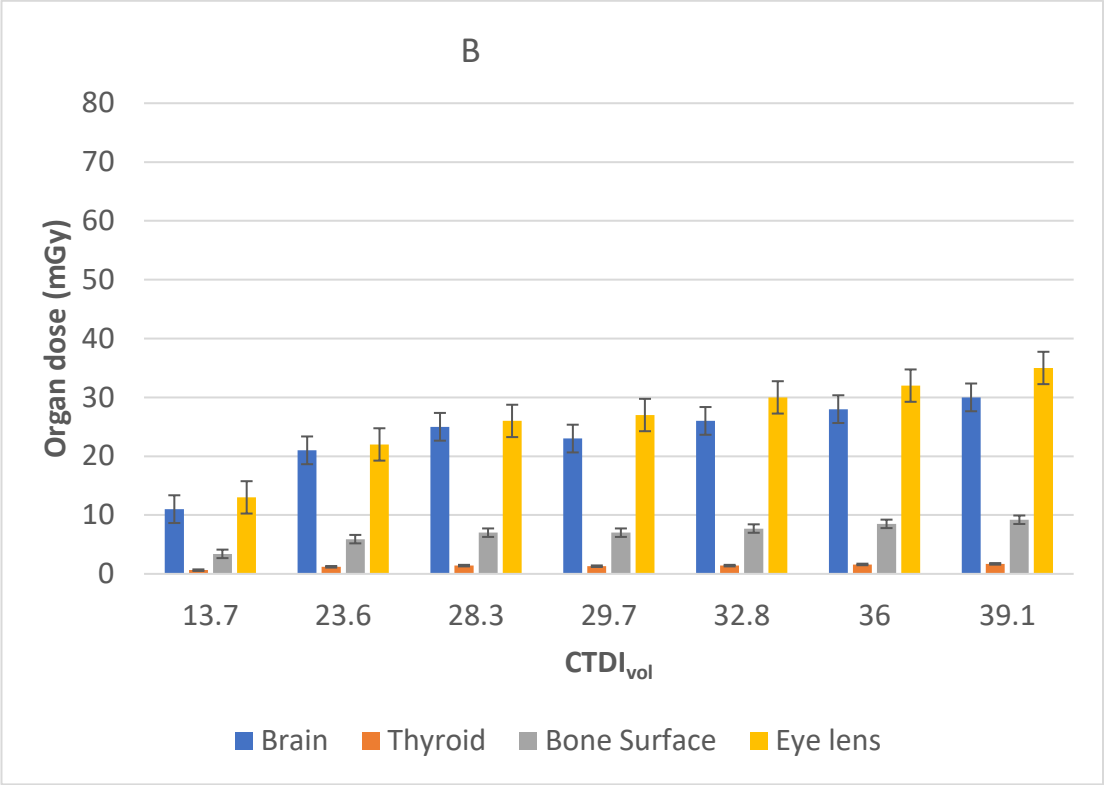

Figure 4.7: A graph of organ dose and $CTDI_{vol}$ using the pitches 0.5 and 0.9.

As shown in Figures 4.7A and 4.7B, the organ dose increased with increasing $CTDI_{vol}$ in both pitches of 0.5 and 0.9. The eye lens received the highest dose while the thyroid received the lowest dose for both pitches. Additionally. It was observed that the 0.9 pitch measured a lower dose of 35 mGy to the eye lens than the 0.5 pitch which measured 63 mGy of dose. It was realised that the higher the pitch the smaller the dose and this might be because of faster table and gantry movement. The ratio of table increments or displacement per 360º rotation to section thickness is the scan pitch value. Dose efficiency increases with smaller slice thickness and the pitch value is also high for small slice thickness. The 0.9 pitch measured a lower dose of 1.3 mGy to the thyroid while the 0.5 pitch measured the dose of 2.3 mGy.

Moreover, it was observed from Figures 4.7A and 4.7B that, there was an average of 45.0% reduction in organ doses when the pitch was changed from 0.5 to 0.9. Even

though the tube voltage and tube current were changed, the eye lens received the highest dose. This is consistent with the findings from (Roslee et al., 2020), who reported that the eye lens consistently received the highest cumulative dose when compared with the other organs.

CHAPTER FIVE

5 CONCLUSIONS AND RECOMMENDATIONS

5.1 CONCLUSION

This research work addressed the assessment of image quality for the set of protocols by measuring noise, contrast to noise ratio, modulation transfer function and noise power spectrum and study the effect on radiation dose.

From the results of this study the eye lens received the highest radiation dose while the thyroid received the least radiation dose.

The 0.9 pitch measured a lower radiation dose than the 0.5 pitch with a percentage reduction of 2.3% and since a shorter gantry and table movement time are used.

The results obtained in this work showed that the H30 kernel (smooth kernel) gave higher values for noise and CNR than the H60 (sharp kernel) which values were also high for the MTF and NPS.

There was an increased in image noise and radiation dose as mAs increased.

Comparing the results of image quality of MTF, noise and CNR with the radiation dose ($CTDI_{vol}$), CNR increased steadily as the $CTDI_{vol}$ increase and noise decreased as the $CTDI_{vol}$ increase.

5.2 RECOMMENDATIONS

The following recommendations are made:

1. It is recommended to the owners of diagnostic facilities to create child friendly environment. And should conduct regular auditing of patient radiation dose and image quality in other to explore more options of optimizing protocols.
2. The radiologist, medical physicist and the radiographer should work as a team to make sure that the ALARA principle is achieved.
3. The computer algorithm used in this work was the filtered back projection. Further study could be done with the iterative reconstruction to investigate if similar results would be attained.

REFERENCES

AAPM. (2011). AAPM position Statement on Radiation Risks from Medical Imaging Procedure (Policy 25-A). *American Association of Physicists in Medicine*.

AAPM. (2013). CT Protocol Management and Review Practice Guideline. *JOURNAL OF APPLIED CLINICAL MEDICAL PHYSICS, Volume 14, Issue 5*.

Aggarwal, L. m. (2014). Biological Effects of Ionizing Radiation. *researchgate, 289952513*.

Akhtar, I. (2016). Research Design. *researchgate, pp17*.

Alexiou, G., Sfakianos, G., & Prodromou, N. (2011). Pediatric head trauma. *J Emeng Trauma Shock, 4:403*.

Alshipli, M., & Kabir, a. n. (2017). Effect of slice thickness on image noise and diagnotic content of single-source-dual energy computed tomography. *Jounal of Physics, 851012005*.

Alsleem, H., & Davidson, R. (2013). Factors Affecting Contrast-Detail Performance in Computed Tomography: A Review. *Journal of Medical Imaging and Radiation Sciences, 44*.

Amis, E. S., Butler, P. F., & Applegate, K. E. (2007). American Colege of Radiology White paper on radiation dose in medicine. *Journal of the American College of Radiology, 4:272-284*.

Andersen, H. K., Volgyes, D., & Martinsen, A. C. T. (2018). Image quality with iterative reconstruction techniques in CT of the lungs-A phantom study. *Eur J Radiol Open, 5,* 35-40. doi:10.1016/j.ejro.2018.02.002

Araki, T., Yokota, H., & Morita, A. (2017). Pediatric Traumatic Brain Injury: Characteristics Features, Diagnosis and Management. *Neurol. Med. Chir., 57(2):82-93*.

Arthurs, J., Rijn, R., Granata, C., Porto, L., Hirsch, F., & Rosendahl, K. (2019). European Society of Paediatric Radiology 2019 strategic research agenda: improving imaging for tomorrow's children. *Pediatric Radiology, 49*.

Berenner, D. J. (2002). Estimating cancer risks from pediatric CT: going from qualitative to quantitative. *pediatric Radiol, 32:228-231*.

Berrington de Gonzale. A, Mahesh M, KP, K., HBhargavan M, Lewis R, Mettler F, & C., L. (2009). Projected cancer risks from computed tomographic scans performed in the United States in 2007. *Archives of Internal Medicine, 169: 2071-7*.

Bolus, E. N. (2001). Basic review of radiation Biology and termiology. *journal of nuclear medicine technology, 29,67-73*.

Brenner, D. J., & Hall, E. J. (2007b). Computed Tomography- An increasing source of Radiation Exposure. *The New England journal of Medicine, 357: 2277 - 2284*.

Brisse, H. J. (2009). The relevance of image quality indices for dose optimisation in abdominal multi-detector row CT in children: experimental assessment with pediatric phantoms. *Phys. Med. Biol. 54, 1871*.

Burnham, J. U. (2005). Biological effects. *RADIATION PROTECTION*.

callahan, M. (2011). CT dose reduction in practice. *Pediatr Radiol, 41:488-492*.

Choi, H. R., Kim, R. E., Heo, C. W., Kim, C. W., Yoo, M. S., & Lee, Y. (2018). Optimization of dose and image quality using self-produced phantom with various diameters in pediatric abdominal CT scan. *Optik, 168*, 54-60. doi:10.1016/j.ijleo.2018.04.066

Cohen, L., Manion, L., & Morrison, K. (2007). *Research methods in Education* (6th Edition ed.). London; Routledge Falmer.

Creswell, J. W. (2003). *Research design; qualitative, quantitative and mixed methods approach* (2nd edition ed.). London, : Sage publications Inc, UK.

Desouky, O., Ding, N., & Guangming, Z. (2015). Target and non-targeted effects of ionizing radiation. *Journal of radiation research and applied sciences, 8, 247-254*.

Dowsett, D. J., Kenny, P. A., & Johnston, R. E. (2006). *The physics of diagnostic imaging* (second edition ed.). Britain: Hodder Arnold.

Euclid, S. (2016). *COMPUTED TOMOGRAPHY: Physical Principles, Clinical Applications and Quality Control* (Fourth ed.). United States of America: Elsevier.

Gao, Y., Quinn, B., Mahmood, U., Long, D., Erdi, Y., St. Germain, J., . . . Dauer, L. (2017). A comparison of peadiatric and adult CT organ dose estimation methods doi:10.1186/s12880-017-0199-3

Goldman, L. W. (2007). Principles of CT and CT technology. *J Nucl Med Technol, 35:115-128*.

Greg, M. (2001). X-ray computed tomography. *physEd, S0031-9120(01)28564-5*.

Gundogdu, S., Mahmutyazicioglu, K., Ozdemir, H., Savranlar, A., & Asil, K. (2005). Assessment of image quality of a standard and three dose-reducing protocols in adult cranial CT. *Eur Radiol, 15*(9), 1959-1968. doi:10.1007/s00330-004-2550-7

Hagelstein, C., Henzler, T., Haubenreisser, H., Meyer, M., Sudarski, S., Schoenberg, S. O., . . . Weis, M. (2016). Ultra-high pitch chest computed tomography at 70 kVp tube voltage in an anthropomorphic pediatric phantom and non-sedated pediatric patients: Initial experience with 3(rd) generation dual-source CT. *Z Med Phys, 26*(4), 349-361. doi:10.1016/j.zemedi.2015.11.002

Halliday, K., Drinkwater, K., & Howlett, D. (2016). Evaluation of paediatric radiology services in hospitals in the UK. *Clin Radiol, 71:1263-1267*.

Hochstadter, E., Stewart, T., Ibrahim, M., & Ranger, A. (2014). Subarachnoid Hemorrhage Prevalence and Its Association with Short-Term Outcome in Pediatric Severe Traumatic Brain Injury. *Nueurocritical Care*.

Hopkins, K. L., Petterson, D. R., & Koudelka, C. W. (2013). Size-appropriate radiation doses in pediatric body CT: a study of regional community adoption in the United States. *Pediatr Radiol, 43(9), 1128-1235*.

Hsieh, J., Nett, B., Yu, Z., Sauer, K., Thibault, J. B., & Bouman, A. C. (2013). Recent Advances in CT Image Reconstruction. *Current Radilogy Reports, 39-51(2013)*.

ICRP. (2007). The 2007 recommendations of the International Commission on Radiological Protection (ICRP, Publication 103). *Annals of the ICRP, 37 (2-4)*.

IMV. (2012). *IMV 2012 CT Market Outlook Report.* Retrieved from

Inkoom, S., Raissaki, M., Perisinakis, K., Maris, T. G., & Damilakis, J. (2015a). Location of radiosensitive organs inside paediatric anthropomorphic phantoms: Data required for dosimetry. *Physica Medica, 882-888*.

Itanyi, U., & HO, L.-Y. (2017). Computed tomography findings in pediatric traumatic head injury in Abuja, Nigeria. *Afr J Med Health Sci, 16:52-7*.

Jallo, J., & Loftus, C. (2009). Neurotrauma and Critical Care of the Brain. *Thieme Medical Pub*.

Johnson, L. (2017). The Role of the Radiographer in Computed Tomography Imaging. *Society of Radiographers, 978-1-909820-155*.

Kalender, W. A., Buchenau, S., Deak, P., Kellermeier, M., Langner, O., van Straten, M., . . . Wilharm, S. (2008). Technical approaches to the optimisation of CT. *Phys Med, 24*(2), 71-79. doi:10.1016/j.ejmp.2008.01.012

Kim, K. R., Cui, H. Y., Jin, W. Y., Lee, J. S., Kaushhik, N., Kim, J. M., . . . Yoo, C. K. (2005). Beneficial effects of low dose radiation in response to the oncogenic KRAs induced cellular transformation. *scientific Reports, 5(15809), 1-9.*

Kofler, J., Cody, D. D., & L, M. R. (2014). CT Protocol Review and Optimization. *J Am Coll Radiol, 11:267-270.*

Li K, Garrett J, Ge Y, & GH, C. (2014). Statistical model based iterative reconstruction(MBIR) in clinical CT systems. Part ll. Experimental assessment of spatial resolution performance. *medical physics, 41(7):071911*.

Loureiro, C. M. E., Filho, A. L. F., & Lima, F. R. d. A. (2015). A GRAPHICAL IMAGE RECONSTRUCTION ALGORITHM FOR COMPUTED TOMOGRAPHY. *researchgate, 978-85-99141-02-1*.

McCollough, C., Primak, A., Braun, N., Kofler, J., Yu, L., & Christner, J. (2009). Strategies for reducing radiation dose in CT. *Radiol clin North Am, 47(1):27-40*.

McNitt-Gray, M. (2006). Tradeoffs in CT image quality and dose. *Med Phys, 33(6):2154-62*.

McNitt-Gray, M. F. (2002). AAPM/RSNA Physics Tutorial for Residents: Topics in CT. *RadioGraphics, 22*.

Morel, B., Bouette, A., Levy, P., Antoni, G., Chalard, F., Blondiaux, E., & Ducou Le Pointe, H. (2016). Optimization of the pediatric head computed tomography scan image quality: Reducing dose with an automatic tube potential selection in infants. *J Neuroradiol, 43*(6), 398-403. doi:10.1016/j.neurad.2016.03.005

Nagel, H. D. (2007). CT parameters that influence the radiation dose. *researchgate*.

Naumann, D. N., Raven, D., Pallan, A., & Bowley, D. M. (2014). Radiation exposure during paediatric emergency CT: time we took notice? *J Pediatr Surg, 49*(2), 305-307. doi:10.1016/j.jpedsurg.2013.11.044

NCRP. (2009). NCRP, Ionizing Radiation Exposure of the Population of the United States. *NCRP publications*.

Noferini, L., Taddeucci, A., Bartolini, M., Bruschi, A., & Menchi, I. (2016). CT image quality assessment by a Channelized Hotelling Observer (CHO): Application to protocol optimization. *Phys Med, 32*(12), 1717-1723. doi:10.1016/j.ejmp.2016.11.002

O'Brien, W. T., Sr., Care, M. M., & Leach, J. L. (2018). Pediatric Emergencies: Imaging of Pediatric Head Trauma. *Semin Ultrasound CT MR, 39*(5), 495-514. doi:10.1053/j.sult.2018.01.007

Pryse-Philip, W. (2014). Companion to clinical neurology. *Oxford University Press, 9780199710041*.

Raj, K., & Mahapatra, A. (2012). *Traumatic Brain Injury*.

Ramos, S. M. O., Thomas, S., Berdeguez, M. B. T., Vasconcellos de Sá, L., & Sousa, S. A. (2017). Anthropomorphic phantoms-potential for more studies and training in radiology. *Internation journal of radiology & radiation therapy, 2*.

Rogers, L. (2001). Radiation exposure in CT: why so high? *AJR Am J Roentgenol, 177(2):277*.

Romans, L. E. (2011). *COMPUTED TOMOGRAPHY for TECHNOLOGISTS* (P. Sabatini Ed.). Batimore, Maryland: Wolters Kluwer Health|Lippincott Williams & Wilkins

Roslee, M. A. A. M., Shuaib, I. L., Napi, A. F. M., Razali, M. A. S. M., & Osman, N. D. (2020). Cumulative organ dose and effective dose in adult population underwent repeated or multiple head CT examination. *Radiation Physics and Chemistry, 166*. doi:10.1016/j.radphyschem.2019.108465

SCoR. (2013). The role of the radiography workforce in CT imaging. *THE SOCIETY & COLLEGE OF RADIOGRAPHERS, 978-1-906225-39-1*.

Seong, K. M., Jin, W. Y., Lee, S. S., King, J. M., Park, S., & Seo, S. (2016). Is the linear no-threshold dose-response paradigm still necessary for the assessment of health effects of low dose radiation? *Korean medical science, 31,10-23*.

Smith, N. B., & Webb, A. (2011). *Introduction to medical imaging; physics, engineering and clinical application*: Cambridge university press.

Sodhi, K. S., Krishna, S., Saxena, A. K., Sinha, A., Khandelwal, N., & Lee, E. Y. (2015). Clinical application of 'Justification' and 'Optimization' principle of ALARA in pediatric CT imaging: "How many children can be protected from unnecessary radiation?". *Eur J Radiol, 84*(9), 1752-1757. doi:10.1016/j.ejrad.2015.05.030

Sorantin, E., Weissensteiner, S., Hasenburger, G., & Riccabona, M. (2013). CT in children--dose protection and general considerations when planning a CT in a child. *Eur J Radiol, 82*(7), 1043-1049. doi:10.1016/j.ejrad.2011.11.041

Sprawls, P., & Duong, P.-A. T. (2013). EFFECTIVE PHYSICS EDUCATION FOR OPTIMISING CT IMAGE QUALITY AND DOSE MANAGEMENT WITH OPEN ACCESS RESOURCES. *MEDICAL PHYSICS INTERNATIONAL, vol.1, No. 1*.

Stephen, P. P., Fiachra, M., Maria, T., Karl, J., Owen, J. O. C., & Maher, M. M. (2016). Computed Tomography and patient risk: Facts, perception and uncertainities. *world J Radiol, 28; 8(12): 902-915*.

Strauss, K., Goske, M., & Kaste, S. (2010). Image Gently: ten steps you can take to optimize image quality and lower CT dose for paediatric patients. *AJR, 194:868-873*.

Strauss, K., Goske, M., Kaste, S., Bulas, D., Frush, P., Butler, P. F., . . . Applegate, E. (2010). Image Gently: Ten Steps You Can Take to Optimize Image Quality and Lower CTdose for Pediatric Patients. *AJR, 191:868-873*.

Stuart, E. M., & Shanmuganathan, K. (2003). *Imaging in Trauma and Critical Care* (Second Edition ed. Vol. 0-7216-9340-7). Philadelphia: Elsevier Science.

Syed, A., Lone, N., Wani, M., & AS, B. (2007). Clinical management of patients with minor head injuries. *Int J Health Sci, 1:131*.

Sze, R. (2011). Building the pediatric radilogy department of the future. *Pediatr Radiol, 41*.

Thukral, B. (2015). Problems and preferences in paediatric imaging. *Indian Journal of Radiology and Imaging*. doi:10.4103/0971-3026.169466

Trattner, S., Pearson, G. D. N., Chin, C., Cody, D. D., Gupta, R., Hess, C. P., . . . Einstein, A. J. (2014). Standardization and optimization of CT protocols to achieve low dose. *J Am Coll Radiol, 11*(3), 271-278. doi:10.1016/j.jacr.2013.10.016

Triantopoulou, S., & Tsapaki, V. (2017). Does clinical indication play a role in CT radiation dose in pediatric patients? *Phys Med, 41*, 53-57. doi:10.1016/j.ejmp.2017.03.014

Verdun, F. R., Racine, D., Ott, J. G., Tapiovaara, M. J., Toroi, P., Bochud, F. O., . . . Marshall, N. W. (2015). Image quality from CT: From physical measurements to model observers. *Physica Medica, 31(2015)823-843*.

Walter, H. (2016). *Review of Radiologic Physics* (FOURTH EDITION ed.). Philadelphia: Wolters Kluwer.

Weinman, J. P., Mirsky, D. M., Jensen, A. M., & Stence, N. V. (2019). Dual energy head CT to maintain image quality while reducing dose in pediatric patients. *Clin Imaging, 55*, 83-88. doi:10.1016/j.clinimag.2019.02.005

Winslow, F., Hyer, E., Fisher, F., Tien, J., & Hintenlang, E. (2009). Construction of anthropomorphic phantoms for use in dosimetry studies. *JOURNAL OF APPLIED CLINICAL MEDICAL PHYSICS, 10(3):195-204*. doi:10.1120/jacmp.v10i3.2986

XGEckerman, X. (2009). Handbook of anatomical models for radiation. *New York:CRC*.

Yu, L. (2016). Image Reconstruction Techniques. *Image wisely*.

Zarb, F., Rainford, L., & McEntee, M. F. (2010). Image quality assessment tools for optimization of CT images. *Radiography, 16*(2), 147-153. doi:10.1016/j.radi.2009.10.002

Zhang, D., Gao, Y., XGEckerman, X., & Liu, B. (2013). Amethod to acquire CT organ dose map using OSL dosimeters and ATOM anthropomorphic phantoms. *Med Phys, 40:081918-19*.

APPENDIX

Appendix A: Interface of the impactscan dosimetry calculator

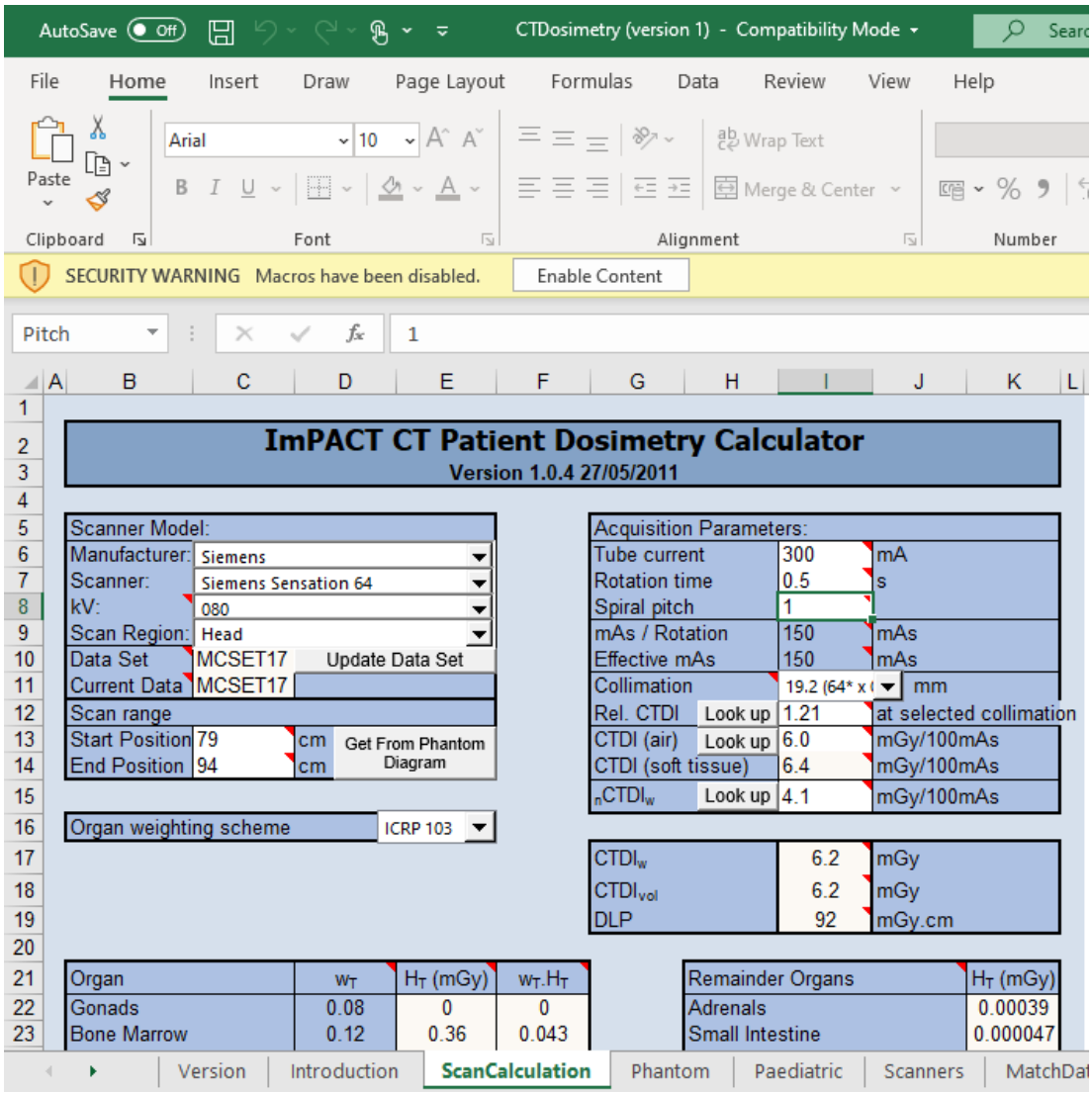

Appendix A

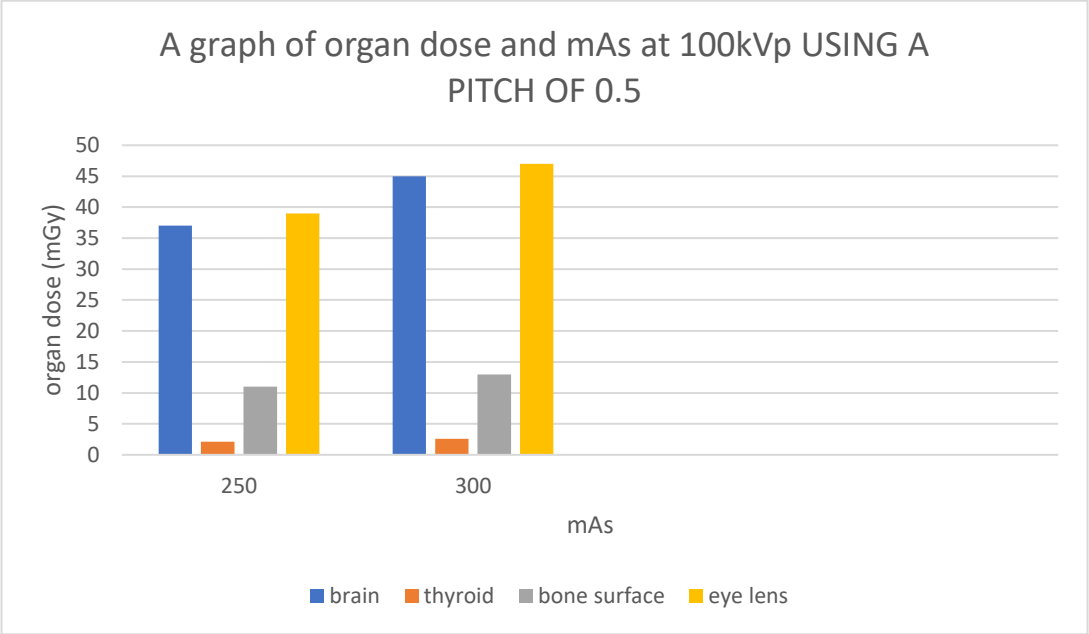

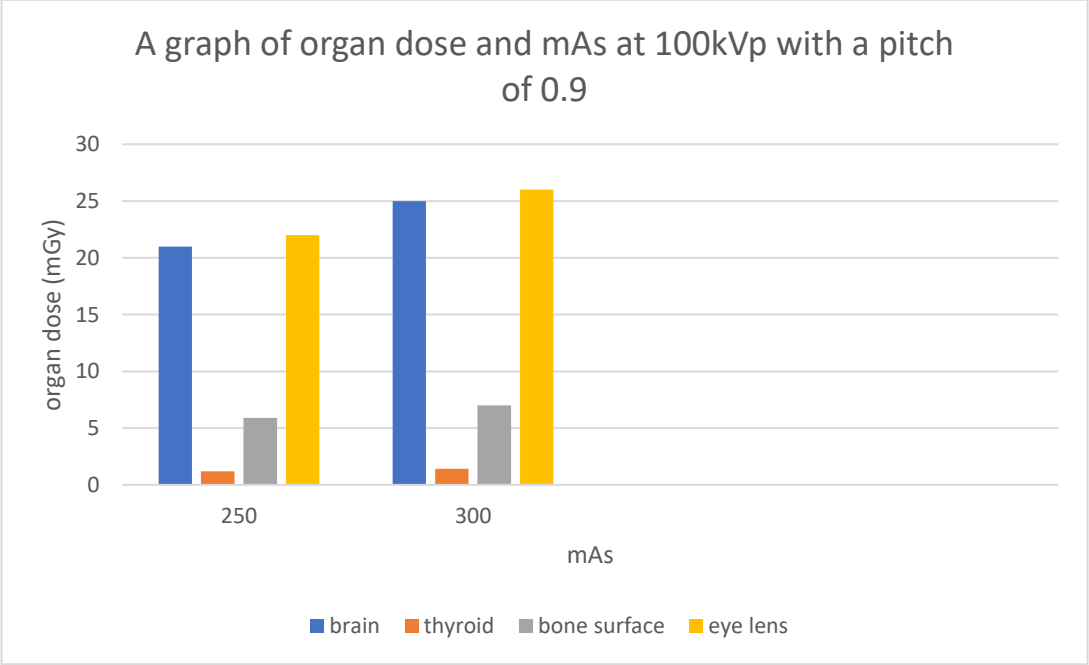

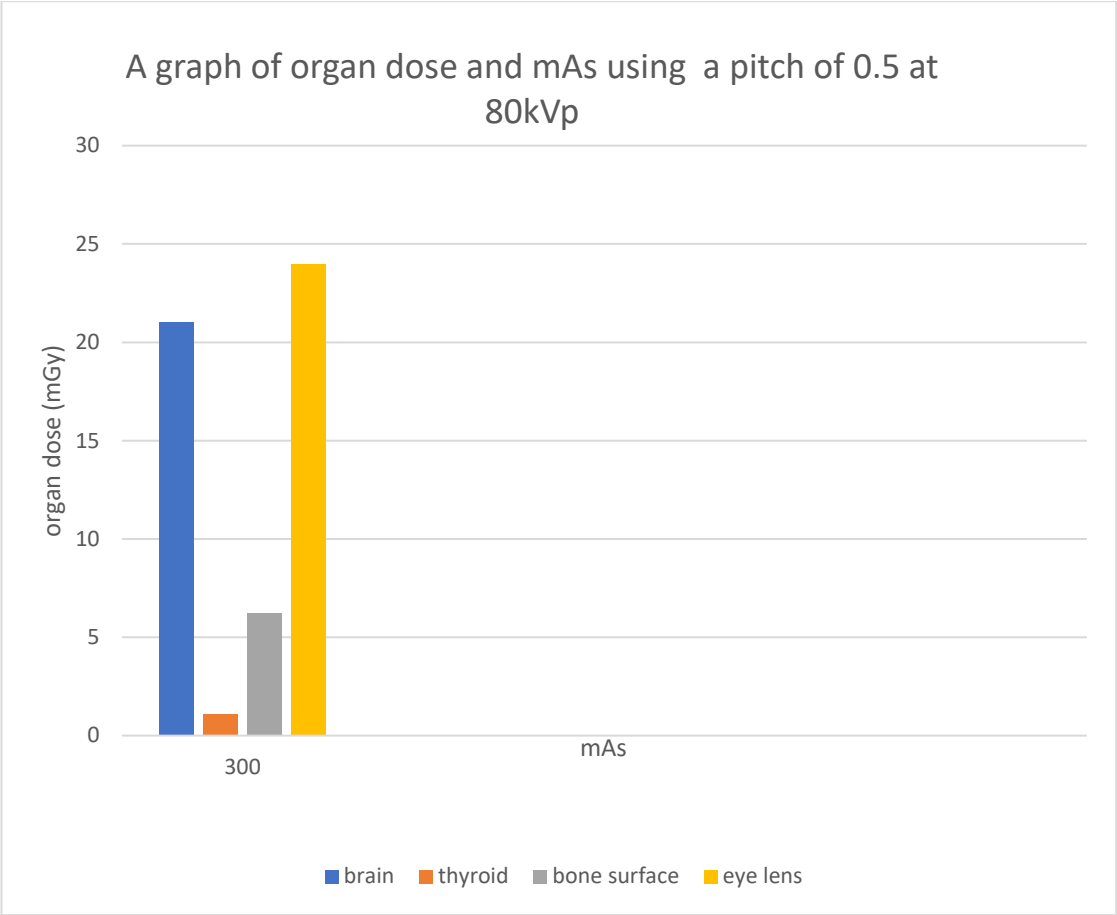

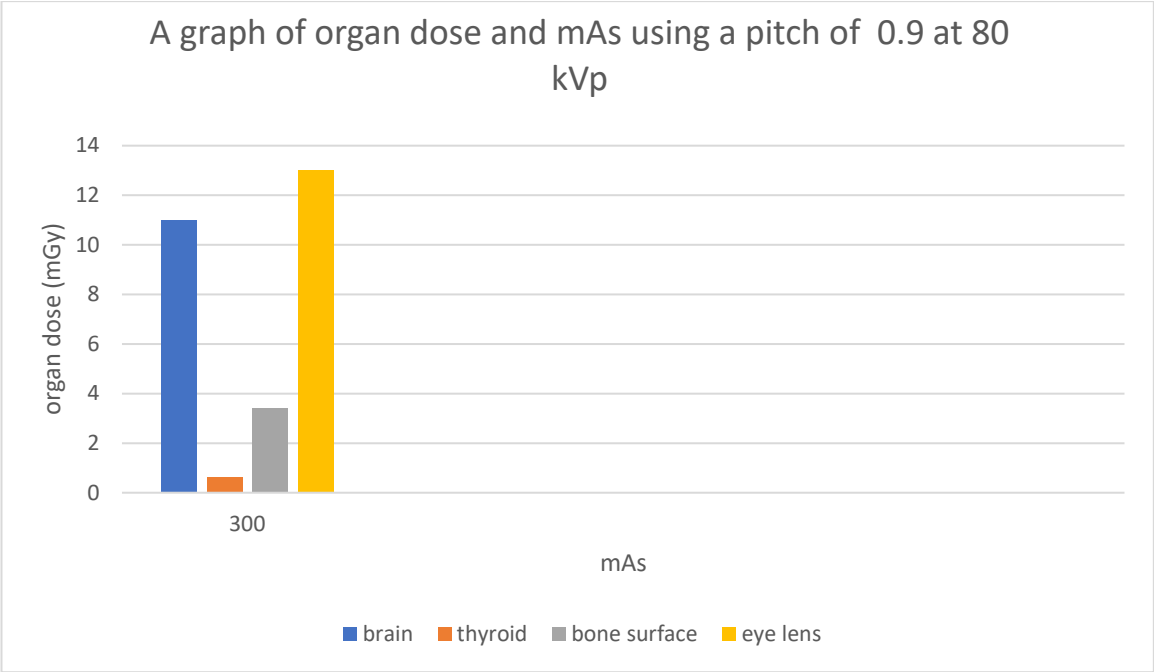

Appendix B: Showing the homogeneity of the phantom

Serial number	Centre	12	15	18	21	Range (HU)
11	11.05	11.27	11.04	10.83	11.25	0.44
12	10.63	10.86	10.59	10.75	10.95	0.36
14	10.78	11.12	11.02	10.84	11.04	0.34
15	10.70	10.81	10.56	10.15	10.14	0.67
16	10.86	11.14	10.91	10.82	11.12	0.32
17	10.56	10.68	10.29	10.29	10.30	0.40
18	11.11	10.10	10.77	10.59	10.93	0.52
19	11.08	10.29	10.26	10.38	10.60	0.83
20	10.77	11.13	10.91	10.71	10.93	0.42
21	11.05	10.84	10.72	10.36	10.38	0.69
22	11.14	10.93	10.67	10.66	10.89	0.48
23	10.10	10.42	10.23	10.29	10.56	0.76
24	10.86	10.89	10.68	10.46	10.91	0.45
25	11.39	10.44	10.64	10.04	10.15	1.34
26	11.17	10.80	10.90	10.43	10.72	0.74
27	10.40	10.33	10.51	10.16	10.00	0.51
28	1.80	1.33	1.41	1.06	1.72	0.74
29	1.19	0.79	0.52	0.75	0.96	0.67
30	1.18	1.71	1.52	1.21	1.60	0.53
31	1.14	1.44	1.13	0.90	1.10	0.55
32	1.53	1.66	1.41	1.39	1.68	0.29
33	1.42	1.23	1.16	0.62	1.24	0.80
34	1.40	1.47	1.18	1.16	1.7	0.53
35	1.15	0.98	0.81	0.79	1.40	0.60
36	-13.81	-12.97	-13.32	-14.129	-13.91	1.15
37	-13.57	-13.48	-14.22	-14.47	-13.88	0.99
38	-14.45	-14.07	-13.95	-14.00	-13.90	0.55
39	-14.11	-14.36	-13.80	-14.33	-14.29	0.56

Appendix C: A table showing the CT-numbers for the various sensitometry inserts

kVp	Water	Polystyrene	LDPE	PMP	Air	Teflon	sDerlin	Acrylic
80	- 3.42	- 61.601	- 117.133	- 205.164	- 951.676	953.546	324.399	97.894
100	- 0.382	- 43.113	- 102.222	- 184.959	- 961.911	926.379	355.399	111.744
120	- 1.669	- 32.549	- 89.051	- 177.242	- 963.765	911.294	338.451	118.298